# The Stability of Spot Patterns for the Brusselator Reaction-Diffusion System in Two Space Dimensions:

## Periodic and Finite Domain Settings

by

Chang, Yifan

B.Sc., Peking University, 2012

A THESIS SUBMITTED IN PARTIAL FULFILLMENT OF
THE REQUIREMENTS FOR THE DEGREE OF

MASTER OF SCIENCE

in

The Faculty of Graduate and Postdoctoral Studies

(Mathematics)

THE UNIVERSITY OF BRITISH COLUMBIA

(Vancouver)

July 2014

# Abstract

In this thesis, we asymptotically construct steady-state localized spot solutions to the Brusselator reaction-diffusion system in the semi-strong interaction regime characterized by an asymptotically large diffusivity ratio. We consider two distinct settings: a periodic pattern of localized spots in $\mathbf{R}^2$ concentrating at lattice points of a Bravais lattice, and multi-spot solutions that concentrate around some discrete points inside a finite domain. We use the method of matched asymptotic expansions, Floquet-Bloch theory, and the study of certain nonlocal eigenvalue problems to perform a linear stability analysis of these patterns. This analysis leads to a two-term approximation for a certain stability threshold characterized by a zero-eigenvalue crossing. Numerical results for the stability threshold are obtained, and compared with various approximations. For the periodic problem, a key feature for the determination of the stability threshold is to use an Ewald summation method to derive an explicit expression for the regular part of the Bloch Green function. Moreover, such an expression allows for the identification of the lattice that offers the optimum stability threshold. For the finite domain problem, we implement our asymptotic theory by calculating the stability threshold for an $N$-spot pattern where the spots are equidistantly spaced on a circular ring that is concentric within the unit disk.

# Table of Contents

# List of Tables

# List of Figures

# Acknowledgements

I would like to thank Dr. Michael Ward and Dr. Juncheng Wei for their great guidance and generous support. I also want to thank all my friends here at UBC who have made these two years a wonderful experience for me. In the end I want to thank my parents for their love through all these years.

# Dedication

To Lionel Messi, the Spain national football team and the beautiful Tiki-taka.

# Chapter 1

# Introduction

Inspired by the work of Allan Turing [14] in 1952, there has been much effort over the past five decades in trying to characterize various patterns that appear in the physical world through the modeling and analysis of reaction-diffusion (RD) systems. In [14], Turing proposed a mechanism for biological morphogenesis based on his analytical study of a coupled two-component system of reaction-diffusion equations with very different diffusion coefficients. Using a linear stability analysis, he found that a small perturbation to a spatially homogeneous initial data can develop into certain spatial patterns through an instability. In the current literature, this type of instability is now referred to as a Turing instability. Since then, various RD systems have been proposed and analyzed to model both biological and chemical patterns. Such systems include the Gray-Scott model (cf. [7]), and the Gierer-Meinhardt system (cf [6]).

Spatially localized spot patterns have been observed both in chemical and numerical experiments. A survey of such patterns is given in [15]. Over the past decade there has been a considerable focus on developing a theoretical mathematical framework for the study of localized patterns for singularly perturbed reaction diffusion systems for which the ratio $\mathcal{O}(\epsilon^{-2})$ of the two diffusivities is asymptotically large. The work of [17] gives a review on the existence, classification and stability of multiple-peaked solutions for the Gierer-Meinhardt system on an interval $I \subset \mathbf{R}^1$. The study [16] generalizes the results to spike solutions in a finite domain $\Omega \subset \mathbf{R}^2$. In both papers, the existence of the multi-peaked solutions is proved rigorously by using the Lyapunov-Schmidt reduction method, while the stability results on the so-called large eigenvalues with $\lambda = \mathcal{O}(1)$ as $\epsilon \to 0$ are based on the study of certain nonlocal eigenvalue problems. In [3] formal singular perturbation

techniques, based on the method of matched asymptotic expansions, are used to analyze the stability of spot patterns for the 2-D Gray-Scott system. In this work, the slow dynamics of the spot patterns is also characterized. The study [10] analyzes the self-replication process of spot patterns for the Schnakenburg model. A formal asymptotic analysis is used to derive an ODE system describing the slow dynamics of the spot patterns, which has the same effect of summing infinite logarithmic series in powers of $\nu = -1/\ln\epsilon$.

In this thesis, we construct localized spot solutions to the 2-D Brusselator in the semi-strong interaction regime characterized by an asymptotically large diffusivity ratio. We then study the stability of these localized patterns. The Brusselator, proposed by Prigogine and co-workers in Brussels in 1960s, is a theoretical model for a hypothetical autocatalytic reaction (cf. [12]). The standard form of this model can be written in terms of non-dimensional space variables as

$$U_T = \epsilon_0^2\Delta U + E - (B+1)U + U^2V\,, \qquad V_T = D\Delta V + BU - U^2V\,, \tag{1.1}$$

where $\epsilon_0^2 = D_u/L^2$, $D = D_v/L^2$, $L$ is a characteristic length-scale, while $D_u$ and $D_v$ are the diffusivities of $U$ and $V$. Many different patterns have been observed for this model through full scale numerical studies of the PDE, and via Turing-type stability analysis augmented by weakly nonlinear theories for the evolution of small amplitude patterns.

Our goal in this thesis is to construct localized spot solutions under the singularly perturbed limit $\epsilon_0 \to 0$ when $E = \mathcal{O}(\epsilon_0)$, while maintaining an asymptotically large diffusivity ratio $D_v/D_u = \mathcal{O}(\epsilon_0^{-2})$, so that $D = D_v/L^2 = (D_v/D_u)(D_u/L^2) = \mathcal{O}(1)$. Then, upon writing $E = \epsilon_0 E_0$ with $E_0 = \mathcal{O}(1)$, $T = t/(B+1)$, $U = Bu/\epsilon_0$, and $V = \epsilon_0 v$ as in [13], the singularly perturbed RD system becomes

$$u_t = \epsilon^2\Delta u + \epsilon^2 E - u + fu^2v\,, \qquad \tau v_t = \mathcal{D}\Delta v + \frac{1}{\epsilon^2}(u - u^2v)\,. \tag{1.2}$$

where we have defined $f$, $\tau$, $E$, $\mathcal{D}$, and $\epsilon$, by

$$f \equiv \frac{B}{B+1}\,, \quad \tau \equiv \frac{1}{f^2}\,, \quad E \equiv \frac{E_0}{B}\,, \quad \mathcal{D} \equiv \frac{D(B+1)}{B^2}\,, \quad \epsilon \equiv \frac{\epsilon_0}{\sqrt{B+1}}\,,$$

This system has three independent bifurcation parameters $E$, $\mathcal{D}$, and $f$, depending on $D$, $B$, and $E_0$. From the definition of $f$, we observe that $f \in (0,1)$.

In order to solve the system (1.2), we still need some information about the domain and boundary conditions. We will consider two cases in this thesis; periodic solutions on $\mathbf{R}^2$ and multi-spot solutions on a finite domain.

For the periodic case, we look for periodic solutions to (1.2) with respect to some Bravais lattices, i.e.

$$u(\boldsymbol{x}+\boldsymbol{l}_i) = u(\boldsymbol{x}), \qquad v(\boldsymbol{x}+\boldsymbol{l}_i) = v(\boldsymbol{x}), \qquad i = 1,2, \tag{1.3}$$

where $\boldsymbol{l}_i, i = 1,2$ are two Bravais vectors. The study [8] undertakes a similar analysis for the Gierer-Meinhardt and Schnakenburg reaction-diffusion systems. Some basic facts concerning Bravais lattices, the Wigner-Seitz primitive cell, reciprocal lattices and Brillouin zones are reviewed in Chapter 2. Due to the periodicity, we can avoid solving the system on the whole plane. Instead, to construct an equilibrium, or steady-state solution, we need only consider a Wigner-Seitz primitive cell together with periodic boundary conditions on the boundary of the cell. After constructing periodic solutions in the primitive cell using the method of matched asymptotic expansions, we perturb this solution and perform a linear stability analysis. The solutions we construct are stable for small $D$, unstable for $D$ large, and the stability threshold occurs when $D \sim \mathcal{O}(\ln \frac{1}{\epsilon})$. To calculate the stability threshold, we need to find the spectrum of the singularly perturbed eigenvalue problem on the whole plane, which is equivalent to finding the eigenfunction of the operator $\Delta + V(\boldsymbol{x})$, where $V(\boldsymbol{x})$ is a periodic function with respect to the Bravais lattices. In this way, the Floquet-Bloch theory arises naturally in the formulation of the stability problem. We prove some basic facts regarding the Bloch Green function in Section 2.3. According to the Floquet-Bloch

theory, instead of solving the perturbed system on the whole plane, we only need to solve it within the the Wigner-Seitz primitive cell with the Bloch quasi-periodic boundary conditions, which involve a Bloch vector $\boldsymbol{k}$ (not unique) in the first Brillouin zone. By analyzing this problem using the method of matched asymptotic expansions, we derive a nonlocal eigenvalue problem. From this problem we obtain the leading order result for the stability threshold, which is independent of the geometry of the lattice and the Bloch vector. To determine a higher-order approximation for the stability threshold, we perform a more refined perturbation analysis in order to calculate a real-valued band of continuous spectrum lying within an $\mathcal{O}(\nu)$ neighbourhood of the origin in the spectral plane. This band does depend on the geometry of the lattice and the Bloch vector $\boldsymbol{k}$. For a given lattice, we determine the next term in the stability threshold from the requirement that the rightmost edge of the real-valued continuous band of spectrum lie in the left plane $\{\lambda|\mathrm{Re}(\lambda) \leq 0\}$ for any Bloch vector $\boldsymbol{k}$ in the first Brillouin zone. This calculation involves minimizing the regular part of the Bloch Green's function. Then, we can determine the optimal lattice arrangement which allows for the largest stability threshold. Overall, the identification of the optimal stability threshold is through a min-max argument. Finally, in addition to this detailed way to calculate the stability threshold, which involves calculating a continuous band of spectrum near the origin of the spectral plane, we also give a quick, but formal, alternative derivation of the first two terms of the stability threshold in Section 3.3.

Our second problem concerns the analysis of the multi-spot patterns to (1.2) on a finite domain $\Omega \subset \mathbf{R}^2$ with the no-flux boundary conditions:

$$\partial_{\boldsymbol{n}} u(\boldsymbol{x}) = 0\,, \qquad \partial_{\boldsymbol{n}} v(\boldsymbol{x}) = 0 \qquad \boldsymbol{x} \in \partial\Omega\,. \tag{1.4}$$

Here $\boldsymbol{n}$ is the outer normal vector on the boundary. We focus on both the existence and linear stability of multi-spot patterns for this problem. The study [13] analyzes a similar problem on a sphere for the Brusselator. We construct asymptotic spot solutions whose $u$ component concentrates on $N$ given points $\boldsymbol{x}_1, \boldsymbol{x}_2, ..., \boldsymbol{x}_n \in \Omega$. For simplicity, we will only consider the case

for which these $N$ spots have a common height. As shown in [16] for the related Gierer-Meinhardt system, the true steady-state positions of these $N$ points are not arbitrary but rather are close to the critical point of a certain objective function related to the Neumann Green function. It is anticipated that a similar result should hold for the true steady-state spot locations for the Brusselator. In our approach, we focus not only on steady-state solutions, but also on quasi steady-state solutions that can persist over very long time intervals. Our only key assumption is that the spot pattern has sufficient symmetry so that the vector $\boldsymbol{e} = (1, 1, ..., 1)^T$ is an eigenvector of a certain Neumann Green's matrix. When this requirement is met, there is a common local behavior near each of the spots. After constructing asymptotic solutions that have this symmetry, we introduce a perturbation and perform a linear stability analysis of these patterns as for the periodic case. The key difference between the periodic and finite domain problems is that, instead of solving the system only within one primitive cell in the periodic case, the interaction of the spots for the finite domain problem arises through a Neumann Green matrix. A detailed calculation of the stability threshold for this problem, based on the method of matched asymptotic expansions, involves the eigenvalues and eigenfunctions of the Neumann Green matrix in an essential way.

The last chapter of this thesis is concerned with performing a few numerical experiments. Firstly, we numerically calculate a key term $\chi(S, f)$, which appears in the boundary conditions when solving the inner core problems near a spot. The numerical results for this quantity are compared with asymptotic approximations for it that are derived in the small source strength limit $S \ll 1$. Then we calculate the stability threshold directly from a nonlinear algebraic equation, and we compare the results with one- and two-term asymptotic approximations. For the periodic problem, we also show that a regular hexagonal lattice of spots offers the optimum stability threshold. Finally, we consider a case study for the finite domain problem, in which $N$ spots are equidistantly-spaced on a circular ring that is concentric with the unit disk. For this configuration, a refined approximation for the stability threshold is calculated.

# Chapter 2

# Preliminaries: The Bravais Lattice and the Bloch Green's Function

## 2.1 Bravais Lattice

In this section we review some basic definitions and results regarding the Bravais lattice. The Bravais lattice was first introduced to describe the periodicity of crystalline solids. The lattice points of a Bravais lattice in $R^d$ can be represented as

$$\Lambda = \{\sum_{i=1}^{d} n_i \boldsymbol{l}_i | n_i \in \mathbf{Z},\ \boldsymbol{l}_i \text{ are linear independent in } \mathbf{R}^d,\ i = 1, 2, ..., n\}, \tag{2.1}$$

so that the lattice looks exactly the same when translated by any integer linear combination of $\boldsymbol{l}_i$, which are called lattice vectors. We remark here that the choice of lattice vectors is not unique. In fact, any linear transformation $\{\sum_{j=1}^{n} a_{ij}\boldsymbol{l}_j\}_{i=1}^{n}$ with $\det(a_{ij}) = \pm 1$ will give the same lattice.

**Definition 2.1.1.** *A primitive cell of a Bravais lattice is the smallest region which when translated by all different integer linear combinations of lattice vectors can cover the entire space without overlapping. The Wigner-Seitz primitive cell of a lattice point is a special primitive cell consisting of all points in space that are closer to this lattice point than to any other lattice point.*

As we can see from the definition, the Wigner-Seitz primitive cell of a

certain lattice point is unique while a primitive cell is not. We can determine the Wigner-Seitz primitive cell of a certain lattice point by identifying the smallest region enclosed by all hyperplanes which perpendicularly bisect the line segments between this point and any other lattice point (it is sufficient to only consider the nearby points around the chosen point).

Now we consider the lattice on $\mathbf{R}^2$. A Bravais lattice $\Lambda$ on $\mathbf{R}^2$ is generated by two lattice vectors $\boldsymbol{l}_1$, $\boldsymbol{l}_2$ which are not parallel to each other. Without lose of generality, we may assume $\boldsymbol{l}_1$ is $(1, 0)$, and we can always choose $\boldsymbol{l}_2 = (a, b)$, such that $a \in (0, 1],\ b > 0$ by adding some $k\boldsymbol{l}_1$, for $k \in \mathbf{Z}$, to the original $\boldsymbol{l}_2$. Then we consider the Wigner-Seitz primitive cell of the origin $O$ and show that it is either a hexagon or a rectangle. First of all, due to the central symmetry of the lattice, we know that the boundaries of the Wigner-Seitz primitive cell will come in pairs and so we only need to look at the right-hand side. Next, after some easy observation, it follows that $\boldsymbol{b}_1$ and $\boldsymbol{b}_2$, which is the perpendicular bisector of $\pm\boldsymbol{l}_2$, form part of the boundaries of the Wigner-Seitz primitive cell. The remainder of the boundary arises from some of the perpendicular bisectors of the line segments between the origin and the points of the second column, i.e. $\boldsymbol{l}_1 + k\boldsymbol{l}_2,\ k \in \mathbf{Z}$. It is useful to observe the mid-points of these line segments lie on a line parallel to $\boldsymbol{l}_2$ passing through the mid-point of $OA$ and the distance between two mid-points next to each other is $\frac{|\boldsymbol{l}_2|}{2}$. Since $\boldsymbol{b}_1$, $\boldsymbol{b}_2$ are perpendicular to $\boldsymbol{l}_2$, and the distance between them is $|\boldsymbol{l}_2|$, then for most of the cases only two of these mid-points will lie between them and the corresponding perpendicular bisectors intersecting with $\boldsymbol{b}_1$, $\boldsymbol{b}_2$ form the boundaries of the primitive cell. This is the generic case when the Wigner-Seitz primitive cell is a hexagon. A special case is when one mid-point lies in the middle of $\boldsymbol{b}_1$, $\boldsymbol{b}_2$ and the two mid-points next to it on $\boldsymbol{b}_1$, $\boldsymbol{b}_2$, Then, the perpendicular bisectors corresponding to these three mid-points is the same line which is perpendicular to $\boldsymbol{b}_1$, $\boldsymbol{b}_2$. Thus, in this case the Wigner-Seitz primitive cell will be a rectangle. In conclusion, if we use the polar coordinate to denote the angle between $\boldsymbol{l}_1$ and $\boldsymbol{l}_2$ by $\theta$, and the length of $\boldsymbol{l}_2$ by $r$, then by the assumption we made on $\boldsymbol{l}_2$, we will have $\theta \in (0, \frac{\pi}{2}),\ r \in (0, \frac{1}{\cos\theta})$ and the Wigner-Seitz primitive cell will be a hexagon unless $r = \frac{\cos\theta}{k},\ k \in \mathbf{Z},\ k > 0$. In this latter, degenerate case, the

primitive cell will be a rectangle.

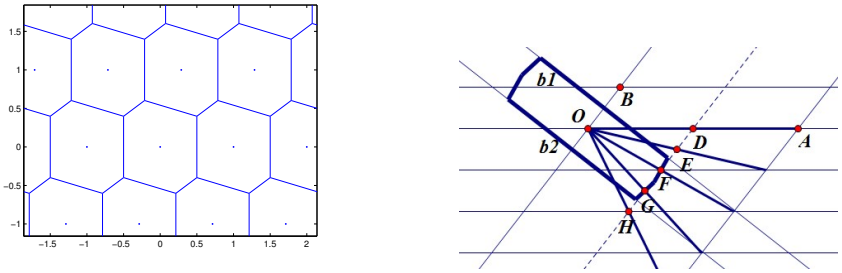


Figure 2.1: Wigner-Seitz primitive cell

## 2.2 Reciprocal Lattice

Next, we review the concept of the reciprocal lattice $\Lambda^*$ of a certain Bravais lattice. This notion arises from Fourier analysis. Firstly, we define a periodic function with respect to a Bravais lattice as follows:

**Definition 2.2.1.** *Given a Bravais lattice $\Lambda$ in $\mathbf{R}^d$ with lattice vectors $\{\boldsymbol{l}_i\}_{i=1}^d$, a function $u(\boldsymbol{x})$ is periodic with respect to the lattice $\Lambda$ if $u(\boldsymbol{x}+\boldsymbol{l}_i) = u(\boldsymbol{x})$, $i = 1, 2, ..., d$.*

We know that a $2\pi$ periodic function $u(x)$ on $\mathbf{R}$ can be decomposed into Fourier series as $e^{inx}$, $n \in \mathbf{Z}$. According to Definition 2.2.1, we can view $u(x)$ as a periodic function with respect to the 1-D lattice $\Lambda = \{n\boldsymbol{l}_1 | n \in \mathbf{Z}, \boldsymbol{l}_1 = 2\pi\}$ and the Fourier basis $e^{inx}$, $n \in \mathbf{Z}$ can be viewed as $e^{\mathrm{i}k\cdot x}$, $k \in \Lambda^* = \{n\boldsymbol{l}_1^* | n \in \mathbf{Z},\ \boldsymbol{l}_1^* = 1\}$, where $\Lambda^*$ is another Bravais lattice related to $\Lambda$, which will be defined as the reciprocal lattice of $\Lambda$ later. In higher dimensions, we first consider a $2\pi$ periodic (in each direction) function $u(\boldsymbol{x})$, i.e. $u(\boldsymbol{x} + 2\pi\boldsymbol{e}_i) = u(\boldsymbol{x})$, $i = 1, 2, ..., d$, where $\boldsymbol{e}_i$ are the standard basis of $\mathbf{R}^d$. We know that $u(\boldsymbol{x})$ can be decomposed into Fourier series of $e^{\mathrm{i}\boldsymbol{n}\cdot\boldsymbol{x}}$, $\boldsymbol{n} \in \mathbf{Z}^d$. As explained above, $u(\boldsymbol{x})$ now can be viewed as a periodic function with respect to the Bravais lattice $\Lambda = \{\sum_{i=1}^d n_i\boldsymbol{l}_i | n_i \in \mathbf{Z},\ \boldsymbol{l}_i = 2\pi\boldsymbol{e}_i,\ i = 1, 2, ..., d\}$. In addition, the Fourier basis $e^{\mathrm{i}\boldsymbol{n}\cdot\boldsymbol{x}}$, $\boldsymbol{n} \in \mathbf{Z}^d$ can be viewed as

$e^{\mathrm{i}\boldsymbol{k}\cdot\boldsymbol{x}}$, $k \in \Lambda^* = \{\sum_{i=1}^d n_i \boldsymbol{l}_i^* | n_i \in \mathbf{Z},\ \boldsymbol{l}_i^* = \boldsymbol{e}_i\}$. For the general case, if $u(\boldsymbol{x})$ is a periodic function with respect to a Bravais lattice $\Lambda$ with lattice vectors $\{\boldsymbol{l}_i\}_{i=1}^d$, we want to decompose it as we did above. In order to convert to the previous case, we use a linear coordinate change $\boldsymbol{x} = \frac{1}{2\pi}[\boldsymbol{l}_1|...|\boldsymbol{l}_d]\boldsymbol{y}$ and denote $A = \frac{1}{2\pi}[\boldsymbol{l}_1|...|\boldsymbol{l}_d]$. Then $\tilde{u}(\boldsymbol{y}) = u(A\boldsymbol{y})$ is a $2\pi$ periodic function in each $y_i$ direction and can be decomposed into Fourier series as $e^{\mathrm{i}\boldsymbol{n}\cdot\boldsymbol{y}} = e^{\mathrm{i}\boldsymbol{n}\cdot(A^{-1}\boldsymbol{x})} = e^{\mathrm{i}((A^{-1})^T\boldsymbol{n})\cdot\boldsymbol{x}}$, $\boldsymbol{n} \in \mathbf{Z}^d$. If we denote $(A^{-1})^T = [\boldsymbol{b}_1|...|\boldsymbol{b}_d]$, then $(A^{-1})^T\boldsymbol{n}$, $\boldsymbol{n} \in \mathbf{Z}^d$, represents a Bravais lattice with lattice vector $\{\boldsymbol{b}_i\}_1^d$. And since $A^T(A^{-1})^T = I$, we have the relation $(\frac{1}{2\pi}\boldsymbol{l}_i)\cdot\boldsymbol{b}_j = \delta_{ij}$, so that $\boldsymbol{l}_i \cdot \boldsymbol{b}_j = 2\pi\delta_{ij}$, which leads to the definition of reciprocal lattice.

**Definition 2.2.2.** *The reciprocal lattice $\Lambda^*$ of a Bravais lattice $\Lambda$ with lattice vectors $\{\boldsymbol{l}_i\}_{i=1}^d$ is the Bravais lattice given by the lattice vectors $\{\boldsymbol{b}_i\}_{i=1}^d$ where $\boldsymbol{b}_i$ are the vectors satisfy $\boldsymbol{l}_i \cdot \boldsymbol{b}_j = 2\pi\delta_{ij}$.*

We remark that $\{\frac{1}{2\pi}\boldsymbol{b}_i\}_{i=1}^d$ are the dual basis for $\{\boldsymbol{l}_i\}_{i=1}^d$ in $\mathbf{R}^d$. Thus, $\{\boldsymbol{b}_i\}_{i=1}^d$ are well defined and uniquely determined by $\{\boldsymbol{l}_i\}_{i=1}^d$. We further remark that other authors choose the reciprocal lattice vectors $\{\boldsymbol{b}_i\}_{i=1}^d$ to satisfy $\boldsymbol{l}_i \cdot \boldsymbol{b}_j = \delta_{ij}$.

Some important properties concerning reciprocal lattices $\Lambda^*$ of a Bravais lattice $\Lambda$ are listed here as follows:

- $\Lambda^* = \{\boldsymbol{b} \in \mathbf{R}^d | e^{\mathrm{i}\boldsymbol{b}\cdot\boldsymbol{l}} = 1,\ \forall \boldsymbol{l} \in \Lambda\}$
- The reciprocal lattice of $\Lambda^*$ is $\Lambda$.
- Any periodic function $u(\boldsymbol{x})$ with respect to $\Lambda$ can be decomposed into Fourier series of $e^{\mathrm{i}\boldsymbol{b}\cdot\boldsymbol{x}}$, where $\boldsymbol{b} \in \Lambda^*$. Using a change of variable, we have the formula:

$$u(\boldsymbol{x}) = \frac{1}{|\Omega|}\sum_{\boldsymbol{b}\in\Lambda^*}\left(\int_\Omega u(\boldsymbol{y})e^{-i\boldsymbol{b}\cdot\boldsymbol{y}}\,d\boldsymbol{y}\right)e^{i\boldsymbol{b}\cdot\boldsymbol{x}}\,. \tag{2.2}$$

- The Fourier transform of $\sum_{\boldsymbol{l}\in\Lambda}\delta(\boldsymbol{x}-\boldsymbol{l})$ is $\frac{(2\pi)^d}{|\Omega|}\sum_{\boldsymbol{b}\in\Lambda^*}\delta(\boldsymbol{\xi}-\boldsymbol{b})$, where $\Omega$ is the Wigner-Seitz primitive cell of $\Lambda$.

- If $u(\boldsymbol{x}) \in L^1(\mathbf{R}^d)$, then $\sum_{\boldsymbol{l}\in\Lambda} u(\boldsymbol{x}+\boldsymbol{l})$ converges absolutely almost everywhere, and we have:

$$\sum_{\boldsymbol{l}\in\Lambda} u(\boldsymbol{x}+\boldsymbol{l}) = \frac{1}{|\Omega|}\sum_{\boldsymbol{b}\in\Lambda^*} \hat{u}(\boldsymbol{b}) e^{\mathrm{i}\boldsymbol{x}\cdot\boldsymbol{b}}\,. \tag{2.3}$$

  In particular, upon replacing $u(\boldsymbol{x})$ by $u(\boldsymbol{x})e^{i\boldsymbol{x}\cdot\boldsymbol{k}}$, we have that

$$\sum_{\boldsymbol{l}\in\Lambda} u(\boldsymbol{x}+\boldsymbol{l}) e^{\mathrm{i}\boldsymbol{k}\cdot\boldsymbol{l}} = \frac{1}{|\Omega|}\sum_{\boldsymbol{b}\in\Lambda^*} \hat{u}(\boldsymbol{b}-\boldsymbol{k}) e^{\mathrm{i}\boldsymbol{x}\cdot(\boldsymbol{b}-\boldsymbol{k})}\,. \tag{2.4}$$

We remark that the last two properties are called Poisson summation formulae. We prove these properties as follows:

*Proof.* First we establish the basic result that the Fourier transform of $\sum_{\boldsymbol{l}\in\Lambda}\delta(\boldsymbol{x}-\boldsymbol{l})$ is $\frac{(2\pi)^d}{V}\sum_{\boldsymbol{b}\in\Lambda^*}\delta(\boldsymbol{\xi}-\boldsymbol{b})$. The key step in the proof is the following equality:

$$\sum_{n=-\infty}^{\infty} e^{\mathrm{i}nx} = 2\pi\sum_{k=-\infty}^{\infty}\delta(x-2\pi k)\,. \tag{2.5}$$

The proof of (2.5) can be found in many books; we simply sketch the outline of the proof here. First of all, the equality holds in the sense of distribution, and since both sides are $2\pi$ periodic, we may prove it only on the interval $[-\pi,\pi]$, i.e. for any test function $\phi(x)\in C_0^\infty[-\pi,\pi]$,

$$\lim_{N\to\infty}\int_{-\pi}^{\pi}(\sum_{n=-N}^{N} e^{\mathrm{i}nx})\phi(x)\,dx = \int_{-\pi}^{\pi}(2\pi\sum_{k=-\infty}^{+\infty}\delta(x-2\pi k))\phi(x)\,dx = 2\pi\phi(0)\,. \tag{2.6}$$

This is true since

$$\sum_{n=-N}^{N} e^{\mathrm{i}nx} = \frac{\sin(N+\frac{1}{2}x)}{\sin\frac{x}{2}} \to \delta(x)\,, \quad \text{as} \quad N\to\infty\,,$$

in the sense of distributions.

Notice that the 1-D case followed directly from this equality,

$$\sum_{n=-\infty}^{\infty} \widehat{\delta(x-nl)} = \sum_{n=-\infty}^{\infty} e^{\mathrm{i}n\cdot\xi l} = 2\pi \sum_{k=-\infty}^{\infty} \delta(l\xi - 2\pi k) = \frac{2\pi}{l} \sum_{k=-\infty}^{\infty} \delta(\xi - k\frac{2\pi}{l})\,.$$

For the higher dimensional case, we have

$$\begin{aligned} \sum_{\boldsymbol{l}\in\Lambda} \widehat{\delta(\boldsymbol{x}-\boldsymbol{l})} &= \sum_{m_i\in\mathbf{Z}} e^{-\mathrm{i}(\sum_{i=1}^{d} m_i\boldsymbol{l}_i)\cdot\boldsymbol{\xi}} = \prod_{i=1}^{d}(\sum_{m_i=-\infty}^{\infty} e^{-\mathrm{i}m_i(\boldsymbol{l}_i\cdot\boldsymbol{\xi})}) \\ &= \prod_{i=1}^{d}(2\pi \sum_{k_i=-\infty}^{\infty} \delta(\boldsymbol{l}_i\cdot\boldsymbol{\xi} - 2\pi k_i)) = \prod_{i=1}^{d}(\sum_{k_i=-\infty}^{\infty} \delta(\frac{\boldsymbol{l}_i\cdot\boldsymbol{\xi}}{2\pi} - k_i))\,. \end{aligned} \tag{2.7}$$

If we denote $\boldsymbol{\xi} = \sum_{i=1}^{d} \eta_i \boldsymbol{b}_i = [\boldsymbol{b}_1|\boldsymbol{b}_1|...|\boldsymbol{b}_d]\boldsymbol{\eta} = B\boldsymbol{\eta}$, where $\{\boldsymbol{b}_i\}_{i=1}^{d}$ are the reciprocal vectors to $\{\boldsymbol{l}_i\}_{i=1}^{d}$, then (2.7) becomes

$$\begin{aligned} &\prod_{i=1}^{d}(\sum_{k_i=-\infty}^{\infty} \delta(\frac{\boldsymbol{l}_i\cdot\boldsymbol{\xi}}{2\pi} - k_i)) = \prod_{i=1}^{d}(\sum_{k_i=-\infty}^{\infty} \delta(\eta_i - k_i)) = \sum_{\boldsymbol{k}\in\mathbf{Z}^d} \delta(\boldsymbol{\eta}-\boldsymbol{k}) \\ &= \sum_{\boldsymbol{k}\in\mathbf{Z}^d} \delta(B^{-1}(\boldsymbol{\xi} - B\boldsymbol{k})) = \frac{1}{\det(B^{-1})} \sum_{\boldsymbol{b}\in\Lambda^*} \delta(\boldsymbol{\xi}-\boldsymbol{b})\,. \end{aligned} \tag{2.8}$$

Since $B^{-1} = \frac{1}{2\pi}[\boldsymbol{l}_1|\boldsymbol{l}_1|...|\boldsymbol{l}_d]$, then $\det(B^{-1}) = \frac{V}{(2\pi)^d}$, where $V = \det([\boldsymbol{l}_1|\boldsymbol{l}_1|...|\boldsymbol{l}_d])$ is the volume of the primitive cell. In this way, we conclude that

$$\sum_{\boldsymbol{l}\in\Lambda} \widehat{\delta(\boldsymbol{x}-\boldsymbol{l})} = \frac{(2\pi)^d}{V} \sum_{\boldsymbol{b}\in\Lambda^*} \delta(\boldsymbol{\xi}-\boldsymbol{b})\,. \tag{2.9}$$

Then we prove the last property. First of all since

$$\int_{\Omega} \sum_{\boldsymbol{l}\in\Lambda} |u(\boldsymbol{x}+\boldsymbol{l})|\,d\boldsymbol{x} = \int_{\mathbf{R}^2} |u(\boldsymbol{x})|\,d\boldsymbol{x} < \infty\,, \tag{2.10}$$

the series $\sum_{\boldsymbol{l}\in\Lambda} u(\boldsymbol{x}+\boldsymbol{l})$ converges absolutely almost everywhere. Moreover, since the series is periodic with respect to the lattice $\Lambda$, then by using the

property above we can decompose it into a Fourier series as

$$\sum_{\boldsymbol{l}\in\Lambda} u(\boldsymbol{x}+\boldsymbol{l}) = \frac{1}{|\Omega|}\sum_{\boldsymbol{b}\in\Lambda^*}\Big(\int_\Omega \Big(\sum_{\boldsymbol{l}\in\Lambda} u(\boldsymbol{y}+\boldsymbol{l})\Big)e^{-i\boldsymbol{b}\cdot\boldsymbol{y}}\,d\boldsymbol{y}\Big)e^{i\boldsymbol{b}\cdot\boldsymbol{x}}\,. \tag{2.11}$$

The last step in the derivation is to calculate the Fourier coefficients as

$$\int_\Omega \Big(\sum_{\boldsymbol{l}\in\Lambda} u(\boldsymbol{y}+\boldsymbol{l})\Big)e^{-i\boldsymbol{b}\cdot\boldsymbol{y}}\,d\boldsymbol{y} = \sum_{\boldsymbol{l}\in\Lambda}\int_\Omega u(\boldsymbol{y}+\boldsymbol{l})e^{-i\boldsymbol{b}\cdot\boldsymbol{y}}\,d\boldsymbol{y} \tag{2.12}$$

$$= \int_{\mathbf{R}^2} u(\boldsymbol{y})e^{-i\boldsymbol{b}\cdot\boldsymbol{y}}\,d\boldsymbol{y} = \hat{u}(\boldsymbol{b})\,, \tag{2.13}$$

where the the second to last equality holds since $\mathbf{R}^2$ is tiled when $\Omega$ translated by all lattice vector, and since $\forall \boldsymbol{l}\in\Lambda$ and $\forall \boldsymbol{b}\in\Lambda^*$, we have $e^{i\boldsymbol{l}\cdot\boldsymbol{b}}=1$.

In particular when we replace $u(\boldsymbol{x})$ by $u(\boldsymbol{x})e^{i\boldsymbol{x}\cdot\boldsymbol{k}}$, the Fourier transform is translated by $\boldsymbol{k}$. □

There are two further useful concepts that relate to Bravais lattices.

**Definition 2.2.3.** *Bragg planes are the hyperplanes which perpendicularly bisect any line segment between two lattice points of $\Lambda^*$. The first Brillouin Zone is the Wigner-Seitz primitive cell of $\Lambda^*$*

## 2.3 Bloch Theorem and Bloch Green Function

In this section, we review Bloch theorem and some properties of the Bloch Green function in the Wigner-Seitz primitive cell $\Omega$ of some lattice $\Lambda$. These results will be used later when we consider the stability of a periodic pattern of spots for the reaction-diffusion system. The proof below is similar to that in [8].

The Bloch theorem originates from quantum mechanics and states that the eigenfunction $\phi(\boldsymbol{x})$ of the operator $-\Delta + V(\boldsymbol{x})$, where the potential function $V(\boldsymbol{x})$ is periodic with respect to a Bravais lattice $\Lambda$, must have the form $\phi(\boldsymbol{x}) = e^{\mathrm{i}\boldsymbol{k}\cdot\boldsymbol{x}}\phi_p(\boldsymbol{x})$, where $\phi_p(\boldsymbol{x})$ is also periodic with respect to the lattice $\Lambda$, and $\boldsymbol{k}$ can be chosen to lie in the first Brillouin Zone, or equivalently $\forall \boldsymbol{l}\in\Lambda$, $\phi(\boldsymbol{x}+\boldsymbol{l}) = e^{\mathrm{i}\boldsymbol{k}\cdot\boldsymbol{l}}\phi(\boldsymbol{x})$. The Bloch theorem allows us

to solve the eigenvalue problem within the primitive cell together with the Bloch boundary conditions, instead of on the whole space. The proof of the Bloch theorem can be found in many solid physics books and the key idea is that if two operators commute, which in this case are $-\Delta + V(\boldsymbol{x})$ and translation by any lattice vector, they share common non-degenerate eigenvectors while the eigenvalues may be different. By using this idea, we can prove the Bloch theorem for a system, which is the basis for our linear stability analysis. Since the equilibrium solutions we construct are periodic with respect to some Bravais lattice $\Lambda$, finding the eigenspace of the linear perturbed system is equivalent to finding the eigenfunction for an operator similar to $-\Delta + V(\boldsymbol{x})$. In this way, the Bloch theorem arises naturally in the stability analysis of a periodic arrangement of spots.

Next we consider some key properties of the Bloch Green function. This is the Green function in the fundamental Wigner-Seitz cell that satisfies the Bloch boundary conditions. As we have shown above, the primitive cell $\Omega$ will be either a hexagon or a rectangle. We may assume that the boundaries of $\Omega$ consist of $\boldsymbol{d}_{\pm i}$, with $i \leq 2$ for a rectangle and $i \leq 3$ for a hexagon, where $\boldsymbol{d}_{\pm i}$ represents the perpendicular bisector of $\pm\boldsymbol{L}_i \in \Lambda$ which come in pairs.

The Bloch Green function in $\Omega$ is the solution to

$$\Delta G_{0,\boldsymbol{k}}(\boldsymbol{x}) = -\delta(\boldsymbol{x}), \qquad \boldsymbol{x} \in \Omega, \tag{2.14}$$

and satisfies the following Bloch boundary conditions, also referred to as quasi-periodic boundary conditions:

$$\begin{aligned} \forall \boldsymbol{x} \in \boldsymbol{d}_{-i}, \qquad & G_{0,\boldsymbol{k}}(\boldsymbol{x} + \boldsymbol{L}_i) = e^{-\mathrm{i}\boldsymbol{k}\cdot\boldsymbol{L}_i} G_{0,\boldsymbol{k}}(\boldsymbol{x}), \\ & \partial_{\boldsymbol{n}-} G_{0,\boldsymbol{k}}(\boldsymbol{x} + \boldsymbol{L}_i) = e^{-\mathrm{i}\boldsymbol{k}\cdot\boldsymbol{L}_i} \partial_{-\boldsymbol{n}+} G_{0,\boldsymbol{k}}(\boldsymbol{x}), \end{aligned} \tag{2.15}$$

where the $\pm$ behind $\boldsymbol{n}$ in the directional derivatives denote one-side derivatives, $\boldsymbol{n}$ is the outer unit normal vector parallel to $\boldsymbol{L}_i$ and $\boldsymbol{k}$ is some non-zero vector in the first Brillouin Zone $\Omega^*$, i.e. in the Wigner-Seitz primitive cell of $\Lambda^*$. We first remark here that we require $\boldsymbol{k} \neq \boldsymbol{0}$ since there is no solution to (2.14) if $\boldsymbol{k} = \boldsymbol{0}$. This is shown by integrating $\Delta G_{0,\boldsymbol{k}}(\boldsymbol{x})$ over $\Omega$, and us-

ing the divergence theorem which results in a contradiction. The boundary conditions are well-defined since $\boldsymbol{x} + \boldsymbol{L}_i \in \boldsymbol{d}_i$ if $\boldsymbol{x} \in \boldsymbol{d}_{-i}$. Moreover, we use one-side normal derivative since we only solve the equation inside $\Omega$. With this boundary conditions, we can extend the solution to the whole plane with continuous normal derivative between contiguous cells.

It is also useful to analyze the quasi-periodic reduced-wave Green's function, which is the solution to

$$\Delta G_{\sigma,\boldsymbol{k}}(\boldsymbol{x}) - \sigma^2 G_{\sigma,\boldsymbol{k}}(\boldsymbol{x}) = -\delta(\boldsymbol{x}), \quad \boldsymbol{x} \in \Omega, \quad \sigma \in \mathbf{R}, \tag{2.16}$$

with the boundary conditions of (2.15). We observe that the Bloch Green function is simply the special case of the reduced-wave Green's function when $\sigma = 0$. The first key property is that the regular part $R_{\sigma,\boldsymbol{k}}$ of $G_{\sigma,\boldsymbol{k}}(\boldsymbol{x})$, which is defined by subtracting the free space Green function $-\frac{1}{2\pi}\ln|\boldsymbol{x}|$ from $G_{\sigma,\boldsymbol{k}}(\boldsymbol{x})$, i.e.

$$R_{\sigma,\boldsymbol{k}} = \lim_{\boldsymbol{x}\to\mathbf{0}} G_{\sigma,\boldsymbol{k}}(\boldsymbol{x}) + \frac{1}{2\pi}\ln|\boldsymbol{x}|,$$

is real for $\boldsymbol{k} \neq \mathbf{0}$.

**Lemma 1.** *The regular part $R_{\sigma,\boldsymbol{k}}$ of $G_{\sigma,\boldsymbol{k}}(\boldsymbol{x})$ is real-valued for $|\boldsymbol{k}| \neq 0$.*

*Proof.* We let $\epsilon > 0$ and eliminate the singularity by cutting a small ball $B(\mathbf{0},\epsilon)$ around the origin. We denote $\Omega_\epsilon \equiv \Omega - B(\mathbf{0},\epsilon)$. Then we use the divergence theorem and the fact that $\Delta G_{\sigma,\boldsymbol{k}}(\boldsymbol{x}) = \sigma^2 G_{\sigma,\boldsymbol{k}}(\boldsymbol{x})$ for $x \in \Omega_\epsilon$ to calculate

$$\begin{aligned}
&\int_{\partial\Omega_\epsilon} \overline{G}_{\sigma,\boldsymbol{k}} \partial_{\boldsymbol{n}} G_{\sigma,\boldsymbol{k}}\, dl = \int_{\partial\Omega_\epsilon} \overline{G}_{\sigma,\boldsymbol{k}} (\nabla G_{\sigma,\boldsymbol{k}} \cdot \boldsymbol{n})\, dl = \int_{\partial\Omega_\epsilon} ((\overline{G}_{\sigma,\boldsymbol{k}} \nabla G_{\sigma,\boldsymbol{k}}) \cdot (\boldsymbol{n}\, dl) \\
&= \int_{\Omega_\epsilon} \nabla \cdot (\overline{G}_{\sigma,\boldsymbol{k}} \nabla G_{\sigma,\boldsymbol{k}})\, d\boldsymbol{x} = \int_{\Omega_\epsilon} \left(\nabla \overline{G}_{\sigma,\boldsymbol{k}} \cdot \nabla G_{\sigma,\boldsymbol{k}} + \overline{G}_{\sigma,\boldsymbol{k}} \Delta G_{\sigma,\boldsymbol{k}}\right) d\boldsymbol{x} \\
&= \int_{\Omega_\epsilon} \left(|\nabla G_{\sigma,\boldsymbol{k}}|^2 + \sigma^2 |G_{\sigma,\boldsymbol{k}}|^2\right) d\boldsymbol{x},
\end{aligned}$$

where $\boldsymbol{n}$ is the outer normal vector as usual. Upon calculating the boundary

integral directly, we have

$$\int_{\partial\Omega_\epsilon} \overline{G}_{\sigma,\boldsymbol{k}} \partial_{\boldsymbol{n}} G_{\sigma,\boldsymbol{k}}\, dl = \int_{\partial\Omega} \overline{G}_{\sigma,\boldsymbol{k}} \partial_{\boldsymbol{n}} G_{\sigma,\boldsymbol{k}}\, dl - \int_{\partial B(\mathbf{0},\epsilon)} \overline{G}_{\sigma,\boldsymbol{k}} \partial_{\boldsymbol{n}} G_{\sigma,\boldsymbol{k}}\, dl\,. \quad (2.17)$$

We claim that the first term vanishes due to the Bloch boundary conditions (2.15). Since $\partial\Omega$ has either 4 or 6 perpendicular bisectors, which come in pairs, then according to (2.15), on each pair $\boldsymbol{d}_{\pm i}$, $G_{\sigma,\boldsymbol{k}}(\boldsymbol{x})$ is different by a factor of $e^{-\mathrm{i}\boldsymbol{k}\cdot\boldsymbol{L}_i}$ and $\partial_{\boldsymbol{n}} G_{\sigma,\boldsymbol{k}}$ is different by $-e^{-\mathrm{i}\boldsymbol{k}\cdot\boldsymbol{L}_i}$ owing to the fact that the outer normal vectors are opposite. Then, if we integrate $\overline{G}_{\sigma,\boldsymbol{k}} \partial_{\boldsymbol{n}} G_{\sigma,\boldsymbol{k}}$ on $\boldsymbol{d}_{\pm i}$, these two terms will be different by $\overline{e^{-\mathrm{i}\boldsymbol{k}\cdot\boldsymbol{L}_i}}(-e^{-\mathrm{i}\boldsymbol{k}\cdot\boldsymbol{L}_i}) = -1$. Thus, the first integral on the right hand-side of (2.17) banishes. Next, we calculate the second term on the right hand-side of (2.17) as

$$\begin{aligned}\int_{\partial B(\mathbf{0},\epsilon)} \overline{G}_{\sigma,\boldsymbol{k}} \partial_{\boldsymbol{x}} G_{\sigma,\boldsymbol{k}}\, d\boldsymbol{x} &\sim \epsilon \int_0^{2\pi} (-\frac{1}{2\pi}\ln\epsilon + \overline{R}_{\sigma,\boldsymbol{k}} + o(1))(-\frac{1}{2\pi\epsilon} + \mathcal{O}(1))\, d\theta \\ &\sim \frac{1}{2\pi}\ln\epsilon - \overline{R}_{\sigma,\boldsymbol{k}} + \mathcal{O}(\epsilon\ln\epsilon)\,.\end{aligned}$$

In this way, we let $\epsilon \to 0$ to obtain

$$\overline{R}_{\sigma,\boldsymbol{k}} = \lim_{\epsilon\to 0}\Big[\int_{\Omega_\epsilon} \left(|\nabla G_{\sigma,\boldsymbol{k}}|^2 + \sigma^2 |G_{\sigma,\boldsymbol{k}}|^2\right)\, d\boldsymbol{x} + \frac{1}{2\pi}\ln\epsilon\Big]\,, \quad (2.18)$$

which proves that $R_{\sigma,\boldsymbol{k}}$ is real-valued. □

As we mentioned before, there is no solution to (2.14) if $\boldsymbol{k} = \mathbf{0}$. So the next lemma will discuss the asymptotic behaviour of $R_{0,\boldsymbol{k}}$ when $\boldsymbol{k}$ tends to $\mathbf{0}$. To analyze this limiting behavior, we may assume $\boldsymbol{k} = \sigma\boldsymbol{\kappa}$, where $\sigma \ll 1$ and $|\boldsymbol{\kappa}| = \mathcal{O}(1)$. This form suggests that we can calculate a solution to (2.14) by a singular perturbation technique. As such, we expand $G_{0,\boldsymbol{k}}$ as

$$G_{0,\boldsymbol{k}}(\boldsymbol{x}) = \frac{U_0(\boldsymbol{x})}{\sigma^2} + \frac{U_1(\boldsymbol{x})}{\sigma} + U_2(\boldsymbol{x}) + \cdots\,. \quad (2.19)$$

In addition, the expansion of the boundary conditions (2.15) yield for $\forall \boldsymbol{x} \in$

$\boldsymbol{d}_{-i}$ that

$$\frac{U_0}{\sigma^2}+\frac{U_1}{\sigma}+...\big|_{\boldsymbol{x}+\boldsymbol{L}_i}=[1-i\sigma(\boldsymbol{\kappa}\cdot\boldsymbol{L_i})+...]\left(\frac{U_0}{\sigma^2}+\frac{U_1}{\sigma}+...\right)\big|_{\boldsymbol{x}}$$
$$\frac{\partial_{\boldsymbol{n}-}U_0}{\sigma^2}+\frac{\partial_{\boldsymbol{n}-}U_1}{\sigma}+...\big|_{\boldsymbol{x}+\boldsymbol{L}_i}=-[1-i\sigma(\boldsymbol{\kappa}\cdot\boldsymbol{L_i})+...]\left(\frac{\partial_{-\boldsymbol{n}+}U_0}{\sigma^2}+\frac{\partial_{-\boldsymbol{n}+}U_1}{\sigma}+...\right)\big|_{\boldsymbol{x}},$$

where $\boldsymbol{n}$ is the outer normal vector on the boundary, which is parallel to $\boldsymbol{L}_i$. Then by equating the same order of $\sigma$, we get:

$$\begin{aligned}
\mathcal{O}(\epsilon^{-2}):\quad & \Delta U_0(\boldsymbol{x})=0\,,\quad \forall\boldsymbol{x}\in\Omega\,,\\
& \forall\boldsymbol{x}\in\boldsymbol{d}_{-i}\,,\quad U_0(\boldsymbol{x}+\boldsymbol{L_i})=U_0(\boldsymbol{x})\,,\quad \partial_{\boldsymbol{n}-}U_0(\boldsymbol{x}+\boldsymbol{L_i})=\partial_{-\boldsymbol{n}+}U_0(\boldsymbol{x})\,.\\
\mathcal{O}(\epsilon^{-1}):\quad & \Delta U_1(\boldsymbol{x})=0\,,\quad \forall\boldsymbol{x}\in\Omega\,,\\
& \forall\boldsymbol{x}\in\boldsymbol{d}_{-i}\,,\quad U_1\big|_{\boldsymbol{x}+\boldsymbol{L}_i}=U_1-i\,(\boldsymbol{\kappa}\cdot\boldsymbol{L}_i)\,U_0\big|_{\boldsymbol{x}}\,,\\
& \partial_{\boldsymbol{n}-}U_1\big|_{\boldsymbol{x}+\boldsymbol{L}_i}=\partial_{-\boldsymbol{n}+}U_1-i\,(\boldsymbol{\kappa}\cdot\boldsymbol{L}_i)\,\partial_{-\boldsymbol{n}+}U_0\big|_{\boldsymbol{x}}\,,\\
\mathcal{O}(1):\quad & \Delta U_2(\boldsymbol{x})=-\delta(\boldsymbol{x})\,,\quad \forall\boldsymbol{x}\in\Omega\,,\\
& \forall\boldsymbol{x}\in\boldsymbol{d}_{-i}\,,\quad U_2\big|_{\boldsymbol{x}+\boldsymbol{L}_i}=U_2-i\,(\boldsymbol{\kappa}\cdot\boldsymbol{L}_i)\,U_1-\frac{(\boldsymbol{\kappa}\cdot\boldsymbol{L}_i)^2}{2}U_0\big|_{\boldsymbol{x}}\,,\\
& \partial_{\boldsymbol{n}-}U_2\big|_{\boldsymbol{x}+\boldsymbol{L}_i}=\partial_{-\boldsymbol{n}+}U_2-i\,(\boldsymbol{\kappa}\cdot\boldsymbol{L}_i)\,\partial_{-\boldsymbol{n}+}U_1-\frac{(\boldsymbol{\kappa}\cdot\boldsymbol{L}_i)^2}{2}\partial_{-\boldsymbol{n}+}U_0\big|_{\boldsymbol{x}}\,.
\end{aligned}$$

From the leading order equation we conclude that $U_0=a$ for some constant $a$. Form the $\mathcal{O}(\epsilon^{-1})$ equation, we get that $U_1$ is a linear function of the form $U_1(\boldsymbol{x})=(-ia\boldsymbol{\kappa})\cdot\boldsymbol{x}+b$, where $b$ is another constant. Next we integrate $\Delta U_2$ over $\Omega$ defined by the $\mathcal{O}(1)$ problem. Upon using the boundary conditions and the expression for $U_0$ and $U_1$, as derived above, we obtain that

$$\begin{aligned}
&\int_\Omega \Delta U_2\,d\boldsymbol{x}=\int_{\partial\Omega}\partial_{\boldsymbol{n}}U_2(\boldsymbol{x})\,dl=\sum_{j=1}^{L}\int_{\pm\boldsymbol{d}_j}\partial_{\boldsymbol{n}}U_2(\boldsymbol{x})\,dl=\int_\Omega -\delta(\boldsymbol{x})\,d\boldsymbol{x}\,,\ \Rightarrow\\
&\sum_{j=1}^{L}-i(\boldsymbol{\kappa}\cdot\boldsymbol{L}_j)\boldsymbol{n}\cdot(-ia\boldsymbol{\kappa})|\boldsymbol{d}_i|=-a\sum_{j=1}^{L}(\boldsymbol{\kappa}\cdot\boldsymbol{L}_j)\frac{\boldsymbol{\kappa}\cdot\boldsymbol{L}_i}{|\boldsymbol{L}_i|}|\boldsymbol{d}_i|=-1\,,
\end{aligned}$$

where $L=2$ if the primitive cell is a rectangle, and $L=3$ if the primitive

cell is hexagon. In this way, we determine $a$ as

$$a = \frac{1}{\sum_{j=1}^{L}(\boldsymbol{\kappa}\cdot\boldsymbol{L}_j)^2\frac{|\boldsymbol{d}_i|}{|\boldsymbol{L}_i|}} = \frac{1}{\boldsymbol{\kappa}^T(\sum_{j=1}^{L}\frac{|\boldsymbol{d}_i|}{|\boldsymbol{L}_i|}\boldsymbol{L}_j\boldsymbol{L}_j^T)\boldsymbol{\kappa}} = \frac{1}{\boldsymbol{\kappa}^T Q\boldsymbol{\kappa}}\,, \tag{2.20}$$

where we denote $Q = \sum_{j=1}^{L}\frac{|\boldsymbol{d}_i|}{|\boldsymbol{L}_i|}\boldsymbol{L}_j\boldsymbol{L}_j^T$. We remark that $Q$ is a positive definite matrix related only to the lattice. This leads to our second lemma:

**Lemma 2.** *For sufficiently small $\boldsymbol{k}$, the regular part $R_{0,\boldsymbol{k}}$ of the Bloch Green function $G_{0,\boldsymbol{k}}$ has the asymptotic behaviour*

$$R_{0,\boldsymbol{k}} \sim \frac{1}{\boldsymbol{k}^T Q\boldsymbol{k}}\,, \tag{2.21}$$

*where $Q$ is a positive definite matrix related to the lattice $\Lambda$ as shown above.*

We remark here that when we try to find the singular perturbed solution $G_{0,\boldsymbol{k}}$ for $\boldsymbol{k}\sim\mathcal{O}(\epsilon)$, the reason we expand $G_{0,\boldsymbol{k}}$ from $\mathcal{O}(\epsilon^{-2})$ is because it can't satisfy the boundary conditions if we start from $\mathcal{O}(\epsilon^{-1})$.

Next we state two other similar results which will be useful later.

**Lemma 3.** *The regular part $R_{\sigma,\boldsymbol{k}}$ of the reduced-wave Bloch Green function $G_{\sigma,\boldsymbol{k}}$ has the asymptotic behaviour $R_{\sigma,\boldsymbol{k}} \sim R_{0,\boldsymbol{k}} + \mathcal{O}(\sigma^2)$, as $\sigma\to 0$ and $|\boldsymbol{k}|\sim\mathcal{O}(1)$, where $R_{0,\boldsymbol{k}}$ is the same as above.*

*Proof.* Just expand $G_{\sigma,\boldsymbol{k}} = G_0 + \sigma^2 G_1 + ....$ Then, we have $G_0$ is the Bloch Green function $G_{0,\boldsymbol{k}}$. And since $G_1$ is bounded for $|\boldsymbol{k}|\sim\mathcal{O}(1)$, we have the asymptotic behaviour $R_{\sigma,\boldsymbol{k}}\sim R_{0,\boldsymbol{k}}+\mathcal{O}(\sigma^2)$. □

**Lemma 4.** *The regular part $R_{\sigma,\boldsymbol{k}}$ of the reduced-wave Bloch Green function $G_{\sigma,\boldsymbol{k}}$ has the asymptotic behaviour $R_{\sigma,\boldsymbol{k}}\sim\frac{1}{\sigma^2[|\Omega|+\boldsymbol{\kappa}^T Q\boldsymbol{\kappa}]}$, as $\sigma\to 0$ and $|\boldsymbol{k}|\sim\mathcal{O}(\sigma)$, where $Q$ is the same positive definite matrix determined by the lattice $\Lambda$.*

*Proof.* The proof is basically the same as we do for $R_{0,\boldsymbol{k}}$, the only difference is the equation for $U_2$ became $\Delta U_2 = U_0 - \delta(\boldsymbol{x})$. So when we integrate $\Delta U_2$, $U_0|\Omega|$ will appear. □

Similar to the Bloch boundary conditions (2.15), we will also use the periodic boundary conditions:

$$G(\boldsymbol{x}+\boldsymbol{l}_i) = G(\boldsymbol{x}), \quad \partial_{\boldsymbol{n}^-} G(\boldsymbol{x}+\boldsymbol{l}_i) = \partial_{-\boldsymbol{n}^+} G(\boldsymbol{x}), \quad \forall \boldsymbol{x} \in \boldsymbol{d}_{-i}, \tag{2.22}$$

# Chapter 3

# Periodic Spot Patterns for the Brusselator

In this chapter we construct periodic spot solutions to (1.2) by first constructing a single spot solution inside the Wigner-Seitz primitive cell $\Omega$ subject to the periodic boundary conditions (2.22). We then periodically extend this solution to the whole plane. Next, we analyze the linear stability of the equilibrium solutions. We first perturb the steady state solution, to derive a singular perturbed eigenvalue problem governing the linear stability of the periodic pattern. From this eigenvalue problem we then provide an accurate calculation of the stability threshold corresponding to a zero eigenvalue crossing. We also provide a more expedient approach to derive the stability threshold.

## 3.1 Periodic Spot Solutions

The Brusselator reaction-diffusion model has the form

$$\begin{aligned} \tilde{u}_t &= \epsilon^2 \Delta \tilde{u} + \epsilon^2 E - \tilde{u} + f\tilde{u}^2\tilde{v}\,, \\ \tau \tilde{v}_t &= D\Delta\tilde{v} + \frac{1}{\epsilon^2}(\tilde{u} - \tilde{u}^2\tilde{v})\,. \end{aligned}$$

From this first equation we observe that there is a spatially homogeneous equilibrium solution for $\epsilon \ll 1$ with $\tilde{u} \sim \epsilon^2 E$, and so we make a substitution of the form $\tilde{u} = u + \epsilon^2 E$ and $\tilde{v} = v$. Then the system becomes

$$\begin{aligned} u_t &= \epsilon^2 \Delta u - u + f(u^2 v + 2\epsilon^2 E u v + \epsilon^4 E v)\,, \\ \tau v_t &= D\Delta v + E + \epsilon^{-2}(u - u^2 v) - 2Euv - \epsilon^2 E^2 v\,. \end{aligned} \tag{3.1}$$

Since the steady-state problem is singularly perturbed, we need to construct a localized asymptotic expansion solutions in the inner region near the origin of the fundamental Wigner-Seitz cell. Then we use the method of matched asymptotic expansions to match the inner solution to an appropriate outer solution.

In the inner region, we use an inner coordinate and perform a scaling to eliminate the $D$. The inner variables $y$, $U$, and $V$, are defined by

$$\boldsymbol{y} = \epsilon^{-1}\boldsymbol{x}\,, \qquad U(\boldsymbol{y}) = \frac{u(\boldsymbol{x})}{\sqrt{D}}\,, \qquad V(\boldsymbol{y}) = \sqrt{D}v(\boldsymbol{x})\,. \tag{3.2}$$

To motivate this scaling of $U$ and $V$, we remark that if we assumed $u \sim D^{\alpha}U$, $v \sim D^{\beta}V$, then from the first equation we have that $\alpha = -\beta = k$, while from the second equation we conclude that $D \cdot \mathcal{O}(D^{-k}) \sim \mathcal{O}(D^{k})$. This leads to $k = 1/2$.

In the inner region, to leading order the solution is radially symmetric. As such, if we denote $\rho = |\boldsymbol{y}|$ then to leading order we get the core problem

$$\Delta_{\rho}U - U + fU^2V = 0\,, \qquad \Delta_{\rho}V + U - U^2V = 0\,, \qquad 0 < \rho < \infty\,, \tag{3.3}$$

where $U$ and $V$ are functions of $\rho$. Therefore, (3.3) is an ODE system. It will have solutions when equipped with initial conditions or appropriate boundary conditions. In this case, we add boundary conditions at $\rho = 0$ and an asymptotic condition as $\rho \to \infty$:

$$U'(0) = V'(0) = 0\,; \quad U \to 0\,, \quad V \sim S\ln\rho + \chi(S,f)\,, \quad \text{as} \quad \rho \to \infty\,, \tag{3.4}$$

where $S$ is some unknown source strength to be determined, while $\chi(S,f)$ is some quantity depending on $S$ and $f$ that is to be computed from the core solution.

We remark here that we choose $U'(0) = V'(0) = 0$ since we are looking for differentiable radically symmetric solutions, $U \to 0$ at infinity since we want localized spot solutions, and we allow $V$ to have logarithmic growth at infinity since the solution to $\Delta V = -\delta(\boldsymbol{y})$ on $\mathbf{R}^2$ is $-\frac{1}{2\pi}\ln|\boldsymbol{y}|$. To derive an

identity for $S$, we integrate $\Delta V$ over $\mathbf{R}^2$ to obtain

$$2\pi S = \int_{\mathbf{R}^2} (U^2V - U)\, d\boldsymbol{x} = \int_0^{2\pi} d\theta \int_0^{\infty} \left(U^2V - U\right) \rho\, d\rho\,,$$

so that

$$S = \int_0^{\infty} \left(U^2V - U\right) \rho\, d\rho\,. \tag{3.5}$$

Next, we construct the outer solution. Since $u$ is localized, the second equation in (3.1) reduces asymptotically to

$$0 = D\Delta v + E + \left( \int_{\Omega} [\epsilon^{-2}(u - u^2v) - 2Euv - \epsilon^2 E^2 v]\, d\boldsymbol{x} \right) \delta(\boldsymbol{x})\,. \tag{3.6}$$

Upon using (3.5), this equation becomes

$$D\Delta v + E = 2\pi S\sqrt{D}\delta(\boldsymbol{x})\,, \qquad \boldsymbol{x} \in \Omega\,. \tag{3.7}$$

Then, if we integrate (3.7) over $\Omega$ and use the periodic boundary conditions on $\partial\Omega$, we can calculate the source strength $S$ as

$$S = \frac{E|\Omega|}{2\pi\sqrt{D}}\,, \tag{3.8}$$

so that (3.7) becomes

$$\Delta v + \frac{E}{D} = \frac{E|\Omega|}{D}\delta(\boldsymbol{x})\,. \tag{3.9}$$

To represent the solution $v$, we introduce the periodic Green function $G_p$ for $\Omega$ as

$$\Delta G_p = \frac{1}{|\Omega|} - \delta(\boldsymbol{x})\,, \quad \boldsymbol{x} \in \Omega\,, \tag{3.10}$$

with the periodic boundary conditions (2.22). Since $G_p$ is determined only up to a constant, we impose that $\int_\Omega G_p\, d\boldsymbol{x} = 0$. As $\boldsymbol{x} \to \mathbf{0}$, $G_p$ has the singular behaviour $G_p \sim -\frac{1}{2\pi}\ln|\boldsymbol{x}| + R_p$, where the regular part $R_p$ can be calculated explicitly for any oblique Bravais lattice, as was shown in [4].

In terms of this Green's function, we have $v = -\frac{E|\Omega|}{D}G_p + c$. As $\boldsymbol{x} \to 0$,

the limiting behavior of $v$ is

$$v \sim \frac{E|\Omega|}{2\pi D} \ln |\boldsymbol{x}| - \frac{E|\Omega|}{D} R_p + c\,. \tag{3.11}$$

We now match this behavior with the inner solution. From (3.4), we obtain as $|\boldsymbol{y}| \to \infty$ that

$$v \sim \frac{1}{\sqrt{D}}(S \ln |\boldsymbol{y}|) + \chi(s,f)) = \frac{E|\Omega|}{2\pi D}(\ln \boldsymbol{x} + \frac{1}{\nu}) + \frac{\chi}{\sqrt{D}}\,, \tag{3.12}$$

where $\nu = \frac{-1}{\ln \epsilon} \ll 1$. Upon matching, we identify the constant $c$ as

$$c = \frac{\chi}{\sqrt{D}} + \frac{1}{\nu}\frac{E|\Omega|}{2\pi D} + \frac{E|\Omega|}{D} R_p\,. \tag{3.13}$$

Since the stability threshold occurs when $D \sim \mathcal{O}(\frac{1}{\nu})$, then from our formula (3.8) for $S$, we conclude that $S \sim \mathcal{O}(\frac{1}{\sqrt{D}}) \sim \mathcal{O}(\nu^{\frac{1}{2}})$. Therefore, for $S = \mathcal{O}(\nu^{1/2})$, we must look for an asymptotic solution to the core problem (3.3). To motivate the scalings for $U$ and $V$, we observe from (3.12) and (3.3) that $V = \sqrt{D}v \sim \mathcal{O}(\frac{1}{\sqrt{D}\nu}) \sim \mathcal{O}(\nu^{-\frac{1}{2}})$, $UV \sim \mathcal{O}(1)$, which leads to $U \sim \mathcal{O}(\nu^{\frac{1}{2}})$. Since $S = \mathcal{O}(\nu^{\frac{1}{2}})$, we need $\chi(S,f)$ to be order $\mathcal{O}(\nu^{-\frac{1}{2}})$ to match with $V$. These formal scaling arguments motivate the following asymptotic expansion for the solution to the core problem:

$$\begin{aligned} &U \sim \nu^{\frac{1}{2}}(U_0 + \nu U_1 + \nu^2 U_2 + \cdots)\,, \qquad V \sim \nu^{-\frac{1}{2}}(V_0 + \nu V_1 + \nu^2 V_2 + \cdots)\,, \\ &\chi \sim \nu^{-\frac{1}{2}}(\chi_0 + \nu \chi_1 + \nu^2 \chi_2 + \cdots)\,, \qquad S \sim \nu^{\frac{1}{2}}(S_0 + \nu S_1 + \nu^2 S_2 + \cdots)\,. \end{aligned} \tag{3.14}$$

Next, we substitute (3.14) into (3.3) and try to construct radially symmetric solutions at each order. At leading order, we have

$$\begin{aligned} &\Delta U_0 - U_0 + f U_0^2 V_0 = 0\,, \quad U_0'(0) = 0\,, \quad U_0 \to 0\,, \quad \text{as} \quad |\boldsymbol{y}| \to \infty\,, \\ &\Delta V_0 = 0\,, \quad V_0'(0) = 0\,, \quad V_0 \to \chi_0\,, \quad \text{as} \quad |\boldsymbol{y}| \to \infty\,. \end{aligned} \tag{3.15}$$

From this system we conclude that

$$U_0 = \frac{\omega}{f\chi_0}\,, \qquad V_0 = \chi_0\,, \tag{3.16}$$

where $\omega$ is the unique positive radially symmetric solution (see [5]) to

$$\Delta\omega - \omega + \omega^2 = 0\,, \tag{3.17}$$

with $\omega(\boldsymbol{y})$ having exponential decay as $|\boldsymbol{y}| \to \infty$. In addition, we have $\int_0^\infty \omega(\rho)\rho d\rho = \int_0^\infty \omega^2(\rho)\rho\, d\rho \equiv b$ upon integrating the equation for $\omega$. Further properties of this ground-state solution are given in [5].

At next order, we have that

$$\Delta U_1 - U_1 + f(\frac{\omega^2}{f^2\chi_0^2}V_1 + 2\frac{\omega}{f}U_1) = \mathcal{L}_0 U_1 + \frac{\omega^2}{f\chi_0^2}V_1 = 0\,, \tag{3.18}$$

$$\Delta V_1 + \frac{\omega}{f\chi_0} - \frac{\omega^2}{\chi_0 f^2} = 0\,, \tag{3.19}$$

$$U_1'(0) = V_1'(0) = 0\,; \quad U_1 \to 0\,, \quad V_1 \to S_0 \ln|\boldsymbol{y}| + \chi_1\,, \quad \text{as} \quad |\boldsymbol{y}| \to \infty\,,$$

where the operator $\mathcal{L}_0$ is defined as $\mathcal{L}_0 u = \Delta u - u + 2\omega u$. By applying the divergence theorem to the $V_1$ equation we obtain that

$$S_0 = \frac{b}{f\chi_0} - \frac{b}{f\chi_0^2} \quad \Rightarrow \quad \chi_0 = \frac{1-f}{f^2}\frac{b}{S_0}\,. \tag{3.20}$$

Then the solutions to (3.18) and (3.19) can be decomposed as

$$U_1 = -\frac{\chi_1}{f\chi_0^2}\omega - \frac{1}{f^3\chi_0^3}U_{1P}\,, \qquad V_1 = \chi_1 + \frac{V_{1P}}{f^2\chi_0}, \tag{3.21}$$

where $U_{1P}$, $V_{1P}$ are the unique radially symmetric solution to

$$\mathcal{L}_0 U_{1P} - \omega^2 V_{1P} = 0\,, \qquad \Delta V_{1P} = \omega^2 - f\omega\,,$$
$$U_{1P}'(0) = V_{1P}'(0) = 0\,; \quad V_{1P} \to (1-f)b\ln|\boldsymbol{y}| + o(1)\,, \quad \text{as} \quad |\boldsymbol{y}| \to \infty\,. \tag{3.22}$$

To eliminate the $f$-dependence in $V_{1P}$, we introduce $V_{1Q}$ satisfying

$$\Delta V_{1Q} = \omega\,, \quad V_{1Q}'(0) = 0\,; \qquad V_{1Q} \to b\ln|\boldsymbol{y}| + o(1)\,, \quad \text{as} \quad |\boldsymbol{y}| \to \infty\,. \tag{3.23}$$

Then we have

$$\Delta(V_{1Q} - \omega) = \omega - \Delta\omega = \omega^2 \quad \Rightarrow \quad V_{1P} = (1-f)V_{1Q} - \omega\,. \tag{3.24}$$

After substituting $V_{1Q}$ into (3.22) we get

$$\mathcal{L}_0 U_{1P} = (1-f)\omega^2 V_{1Q} - \omega^3\,. \tag{3.25}$$

This suggests that we should decompose $U_{1P}$ by introducing $U_{1QI}$ and $U_{1QII}$, which are taken to satisfy

$$\mathcal{L}_0 U_{1QI} = \omega^3\,, \quad U_{1QI}'(0) = 0\,, \quad U_{1QI} \to 0\,, \quad \text{as} \quad |\boldsymbol{y}| \to \infty\,, \tag{3.26}$$

$$\mathcal{L}_0 U_{1QII} = \omega^2 V_{1Q}\,, \quad U_{1QII}^{'}(0) = 0\,, \quad U_{1QII} \to 0\,, \quad \text{as} \quad |\boldsymbol{y}| \to \infty\,, \tag{3.27}$$

so that $U_{1P} = (1-f)U_{1QII} - U_{1QI}$.

At second order we obtain that

$$\begin{aligned}
&\mathcal{L}_0 U_2 + f\Big(\frac{\omega^2}{f^2\chi_0^2}V_2 + \chi_0 U_1^2 + 2\frac{\omega}{f\chi_0}U_1 V_1\Big) = 0\,,\\
&U_2'(0) = 0\,, \quad U_2 \to 0\,, \quad \text{as} \quad |\boldsymbol{y}| \to \infty\,,\\
&\Delta V_2 + U_1 - U_0^2 V_1 - \frac{2\omega}{f}U_1 = 0\,,\\
&V_2'(0) = 0\,, \quad V_2 \to S_1 \ln|\boldsymbol{y}| + \chi_2\,, \quad \text{as} \quad |\boldsymbol{y}| \to \infty\,.
\end{aligned}$$

By using the divergence theorem on the $V_2$ equation we calculate $S_1$ as

$$S_1 = \int_0^\infty U_0^2 V_1 \rho\, d\rho + \frac{2}{f}\int_0^\infty \omega U_1 \rho\, d\rho - \int_0^\infty U_1 \rho\, d\rho\,. \tag{3.28}$$

Next, upon integrating (3.18) we get

$$\int_{\mathbf{R}^2} \mathcal{L}_0 U_1 \, d\boldsymbol{x} + \int_{\mathbf{R}^2} \frac{\omega^2}{f\chi_0^2} V_1 \, d\boldsymbol{x} = 0\,,$$
$$\Rightarrow -\int_0^\infty U_1 \rho \, d\rho + \int_0^\infty 2\omega U_1 \rho \, d\rho + \int_0^\infty \frac{\omega^2}{f\chi_0^2} V_1 \rho \, d\rho = 0\,,$$

where $\int_{\mathbf{R}^2} \Delta U_1 \, d\boldsymbol{x}$ vanishes due to the boundary conditions. Upon substituting this back into (3.28), together with (3.26) and (3.27), we obtain that

$$\frac{f}{1-f} S_1 = \int_0^\infty U_1 \rho \, d\rho = \int_0^\infty (-\frac{\chi_1}{f\chi_0^2}\omega - \frac{1}{f^3\chi_0^3}((1-f)U_{1QII} - U_{1QI}))\rho \, d\rho$$
$$= -\frac{\chi_1 b}{f\chi_0^2} - \frac{1-f}{f^3\chi_0^3}\int_0^\infty U_{1QII}\rho \, d\rho + \frac{1}{f^3\chi_0^3}\int_0^\infty U_{1QI}\rho \, d\rho\,.$$

We then combine this expression with (3.21) and (3.20) to calculate $\chi_1$ as

$$\chi_1 = \frac{f\chi_0^2}{b}(-\frac{1-f}{f^3\chi_0^3}\int_0^\infty U_{1QII}\rho \, d\rho + \frac{1}{f^3\chi_0^3}\int_0^\infty U_{1QI}\rho \, d\rho - S_1\frac{f}{1-f})\,,$$
$$= -\frac{(1-f)b}{f^2}\frac{S_1}{S_0^2} - \frac{S_0}{b^2}\int_0^\infty U_{1QII}\rho \, d\rho + \frac{S_0}{(1-f)b^2}\int_0^\infty U_{1QI}\rho \, d\rho\,.$$

In conclusion, we have constructed a two-term asymptotic spot solution to the core problem (3.3) in the limit $S \to 0$. We summarize our result as follows:

**Principal Result 1.** *For $S \sim \nu^{\frac{1}{2}}(S_0 + \nu S_1 + ...)$, where $\nu \equiv \frac{-1}{\ln \epsilon}$, the core problem (3.3) has an asymptotic solution in the form*

$$U \sim \nu^{\frac{1}{2}}(U_0 + \nu U_1 + \cdots), \quad V \sim \nu^{-\frac{1}{2}}(V_0 + \nu V_1 + \cdots), \quad \chi \sim \nu^{-\frac{1}{2}}(\chi_0 + \nu\chi_1 + \cdots)\,, \tag{3.29}$$

*where $U_0(\rho)$, $U_1(\rho)$, $V_0(\rho)$ and $V_1(\rho)$ are defined by:*

$$U_0 = \frac{\omega}{f\chi_0}\,, \qquad U_1 = -\frac{\chi_1}{f\chi_0^2}\omega - \frac{1}{f^3\chi_0^3}((1-f)U_{1QII} - U_{1QI})\,,$$
$$V_0 = \chi_0\,, \qquad V_1 = \chi_1 + \frac{1}{f^2\chi_0}((1-f)V_{1Q} - \omega)\,.$$

*Here $U_{1QI}$, $U_{1QII}$, and $V_{1Q}$ are the unique radially symmetric solutions to (3.26), (3.27), and (3.24), respectively. In addition, $\omega$ is the unique positive radially symmetric solution to (3.17), while $\chi_0$ and $\chi_1$ are defined by*

$$\chi_0 = \frac{(1-f)}{f^2}\frac{b}{S_0}\,,$$
$$\chi_1 = -\frac{(1-f)b}{f^2}\frac{S_1}{S_0^2} - \frac{S_0}{b^2}\int_0^\infty U_{1QII}\rho\,d\rho + \frac{S_0}{(1-f)b^2}\int_0^\infty U_{1QI}\rho\,d\rho\,.$$

## 3.2 Linear Stability Analysis

In this section, we perform a linear stability analysis for the equilibrium spot solution that we have just constructed. We perturb the steady state solutions and derive the singularly perturbed eigenvalue problem. By analyzing this eigenvalue problem we get the stability threshold. As we mentioned in Section 2.3, since the steady state solutions we have just derived is periodic with respect to the lattice $\Lambda$, solving the perturbed system is equivalent to finding eigenfunctions of the operator $\Delta + f(\boldsymbol{x})$, where $f(\boldsymbol{x})$ is a $2\times 2$ periodic matrix with respect to the lattice $\Lambda$. As a result of the generalized Bloch theory, instead of solving the perturbed system on $\mathbf{R}^2$, we need only consider the eigenvalue problem within the primitive cell $\Omega$ with the Bloch boundary conditions (2.15), which involves a Bloch vector in the First Brillouin Zone.

We begin perturbing the equilibrium solutions as

$$u = u_e + e^{\lambda t}\phi\,, \qquad v = v_e + e^{\lambda t}\eta\,. \tag{3.30}$$

We linearize the equations around this steady state solution and obtain, to leading order, the singularly perturbed eigenvalue problem

$$\lambda\begin{pmatrix}\phi\\ \tau\eta\end{pmatrix} = \begin{pmatrix}\epsilon^2\Delta\phi\\ D\Delta\eta\end{pmatrix} + \begin{pmatrix}-1+2fu_ev_e & fu_e^2\\ \epsilon^{-2}-2\epsilon^{-2}u_ev_e & \epsilon^{-2}u_e^2\end{pmatrix}\begin{pmatrix}\phi\\ \eta\end{pmatrix}, \tag{3.31}$$

for $\boldsymbol{x} \in \Omega$, where $\phi$ and $\eta$ satisfy the Bloch boundary conditions (2.15) for some $\boldsymbol{k}$ in the first Brillouin Zone.

Since the equilibrium solution is localized then, as similar to the construction of the equilibrium spot solution, we introduce an inner region near the core of the spot. As such, we introduce the following inner coordinates and scale the system as

$$\boldsymbol{y} = \epsilon^{-1}\boldsymbol{x}\,, \qquad \Phi(\boldsymbol{y}) = \frac{\phi(\boldsymbol{x})}{D} = \frac{\phi(\epsilon\boldsymbol{y})}{D}\,, \qquad N(\boldsymbol{y}) = \eta(\boldsymbol{x}) = \eta(\epsilon\boldsymbol{y})\,. \quad (3.32)$$

We still look for radially symmetric solutions $\Phi(\boldsymbol{y}) = \Phi(\rho)$, $N(\boldsymbol{y}) = N(\rho)$, where $\rho = |\boldsymbol{y}|$. Then, to leading order, the inner system becomes

$$\Delta_\rho \Phi - (\lambda+1)\Phi + 2fUV\Phi + fU^2 N = 0\,, \quad \Phi'(0) = 0\,; \quad \Phi \to 0 \ \text{ as } \ \rho \to \infty\,, \tag{3.33}$$

$$\Delta_\rho N + (1-2UV)\Phi - U^2 N = 0\,, \quad N'(0) = 0\,; \quad N \to C\ln|\boldsymbol{y}| + B(C,f)\,, \tag{3.34}$$

as $\rho \to \infty$. We remark here that since this is a linear system for a fixed $f$, it follows that the ratio $\frac{B}{C}$ is a constant. In addition, we remark that the asymptotic boundary condition for $\Phi$ is appropriate provided that $\mathrm{Re}(\lambda + 1) > 0$, i.e. that $\lambda$ is not in the continuous spectrum. Finally, we obtain the following identity by integrating the equation for $N$ to get

$$C = \int_0^\infty (U^2 N - (1-2UV)\Phi)\rho\, d\rho\,. \tag{3.35}$$

In terms of $C$, in the outer region the second equation of (3.31) is approximated as

$$\Delta\eta - \frac{\tau\lambda}{D}\eta = 2\pi C\delta(\boldsymbol{x})\,, \tag{3.36}$$

with the Bloch boundary conditions (2.15) for some Bloch vector $\boldsymbol{k}$. In terms of the reduced-wave Bloch Green function (2.16), we can write $\eta$ as

$$\eta = -2\pi C G_{\mu,\boldsymbol{k}}(\boldsymbol{x})\,, \qquad \mu = \sqrt{\frac{\tau\lambda}{D}} \sim \mathcal{O}(\nu^{\frac{1}{2}})\,. \tag{3.37}$$

Therefore, as $\boldsymbol{x} \to \mathbf{0}$, $\eta(\boldsymbol{x})$ has the asymptotic behaviour

$$\eta(\boldsymbol{x}) \sim -2\pi C(-\frac{1}{2\pi}\ln|\boldsymbol{x}| + R_{\mu,\boldsymbol{k}}) \sim C\ln|\boldsymbol{x}| - 2\pi C R_{\mu,\boldsymbol{k}}\,. \tag{3.38}$$

We know from Lemma 3 that if $|\boldsymbol{k}|$ is bounded away from the origin, then we have $R_{\mu,\boldsymbol{k}} = R_{0,\boldsymbol{k}} + \mathcal{O}(\mu^2) = R_{0,\boldsymbol{k}} + \mathcal{O}(\nu)$.

Next, we asymptotically match (3.38) with the far-field behavior of the inner solution (3.34), which is given by

$$\eta \sim C\ln|\boldsymbol{x}| + \frac{C}{\nu} + B\,. \tag{3.39}$$

Upon comparing (3.38) and (3.39), we conclude that

$$C(1 + 2\pi\nu R_{0,\boldsymbol{k}} + \mathcal{O}(\nu^2)) = -\nu B\,. \tag{3.40}$$

Next, we will calculate the asymptotic solution to (3.33) and (3.34) for $\nu$ small. Since we have $UV \sim \mathcal{O}(1)$, $U^2 \sim \mathcal{O}(\nu)$ and $C \sim \nu B$, this suggests that we expand the solutions as

$$\begin{aligned} &\Phi \sim \nu(\Phi_0 + \nu\Phi_1 + \cdots)\,, \qquad N \sim N_0 + \nu N_1 + \cdots\,, \\ &B \sim B_0 + \nu B_1 + \cdots\,, \qquad C \sim \nu(C_0 + \nu C_1 + \cdots)\,. \end{aligned}$$

Upon substituting these expansions into (3.33) and (3.34), we obtain to leading order that

$$\begin{aligned} &\Delta\Phi_0 - (\lambda+1)\Phi_0 + 2fU_0V_0\Phi_0 + fU_0^2N_0 = 0\,, \qquad \Delta N_0 = 0\,, \\ &\Phi_0'(0) = N_0'(0) = 0\,; \qquad \Phi_0 \to 0\,, \qquad N_0 \to B_0 \quad \text{as} \quad |\boldsymbol{y}| \to \infty\,. \end{aligned}$$

Then, upon substituting the expressions for $U_0$ and $V_0$, as given in Principal Result 1, we get

$$\mathcal{L}_0\Phi_0 = \lambda\Phi_0 - \frac{B_0}{f\chi_0^2}\omega^2\,, \qquad N_0 = B_0\,. \tag{3.41}$$

From (3.40), we conclude that

$$B_0 = -C_0 = N_0\,, \qquad B_1 = -C_1 - 2\pi R_{0,\boldsymbol{k}} C_0\,. \tag{3.42}$$

At next order, we have that $\Phi_1$ satisfies

$$\begin{aligned} &\Delta\Phi_1 - (\lambda+1)\Phi_1 + 2f(U_0V_1 + U_1V_0)\Phi_0 + 2fU_0V_0\Phi_1 \\ &\quad + fU_0^2N_1 + 2fU_0U_1N_0 = 0\,; \qquad \Phi_1'(0) = 0\,, \quad \Phi_1 \to 0 \quad \text{as} \quad |\boldsymbol{y}| \to \infty\,, \end{aligned} \tag{3.43}$$

while $N_1$ satisfies

$$\begin{aligned} &\Delta N_1 + (1 - 2U_0V_0)\Phi_0 - U_0^2N_0 = 0\,, \\ &\qquad\qquad N_1'(0) = 0\,, \quad N_1 \to C_0 \ln|\boldsymbol{y}| + B_1 \quad \text{as} \quad |\boldsymbol{y}| \to \infty\,. \end{aligned}$$

Upon substituting the results for $U_0$ and $V_0$ from Principal Result 1, we obtain from the divergence theorem on the $N_1$ equation that

$$C_0 = \left(1 + \frac{b}{f^2\chi_0^2}\right)^{-1} \int_0^\infty \left(\frac{2}{f}\omega - 1\right)\Phi_0\rho\,d\rho\,. \tag{3.44}$$

With $C_0$ now determined, we substitute it back into the equation for $\Phi_0$ to obtain

$$\mathcal{L}_0\Phi_0 = \lambda\Phi_0 + \frac{f}{b + f^2\chi_0^2}\left(\frac{2}{f}\int_0^\infty \omega\Phi_0\rho\,d\rho - \int_0^\infty \Phi_0\rho\,d\rho\right)\omega^2\,. \tag{3.45}$$

In contrast to the nonlocal eigenvalue problems (NLEP's) analyzed in [8], this NLEP is more intricate as it involves two nonlocal terms. In order to obtain an NLEP with only one nonlocal term, we integrate (3.45) to derive

$$\begin{aligned} \int_{\mathbf{R}^2} \mathcal{L}_0\Phi_0\,d\boldsymbol{x} &= 0 - 2\pi\int_0^\infty \Phi_0\rho\,d\rho + 4\pi\int_0^\infty \omega\Phi_0\rho\,d\rho \\ &= 2\pi\lambda\int_0^\infty \Phi_0\rho\,d\rho + \frac{2\pi bf}{b + f^2\chi_0^2}\left(\frac{2}{f}\int_0^\infty \omega\Phi_0\rho\,d\rho - \int_0^\infty \Phi_0\rho\,d\rho\right), \end{aligned}$$

which leads to

$$(\lambda + 1 - \frac{bf}{b + f^2\chi_0^2}) \int_0^\infty \Phi_0 \rho \, d\rho = (2 - \frac{2b}{b + f^2\chi_0^2}) \int_0^\infty \Phi_0 \omega \rho \, d\rho \,. \qquad (3.46)$$

We substitute this back into (3.45) to get

$$\begin{aligned} &\mathcal{L}_0\Phi_0 - \frac{2b(\lambda + 1 - f)}{(\lambda + 1)(b + f^2\chi_0^2) - bf} \frac{\int_0^\infty \Phi_0 \omega \rho \, d\rho}{\int_0^\infty \omega^2 \rho \, d\rho} \omega^2 \\ &= \mathcal{L}_0\Phi_0 - \frac{2(\lambda + 1 - f)}{(\lambda + 1)(1 + (\frac{1-f}{f})^2 \frac{b}{S_0^2}) - f} \frac{\int_0^\infty \Phi_0 \omega \rho \, d\rho}{\int_0^\infty \omega^2 \rho \, d\rho} \omega^2 = \lambda \Phi_0 \,. \end{aligned}$$

To analyze this NLEP we use some previous results on NLEP's similar to the one above, which can be found in [16]. From this previous theory, we know the stability threshold occurs when $\beta(0) = 1$, where $\beta(\lambda)$ is the multiplier of the nonlocal term defined by

$$\beta(\lambda) = \frac{2(\lambda + 1 - f)}{(\lambda + 1)(1 + (\frac{1-f}{f})^2 \frac{b}{S_0^2}) - f} \,.$$

This condition determines a critical value $S_{c0}$ of $S_0$ as $S_{c0}^2 = \frac{(1-f)b}{f^2}$. Then, by (3.8), this determines the following leading order result for the stability threshold:

$$D_c = \frac{D_{c0}}{\nu} + D_{c1} + \cdots \,, \qquad D_{c0} = \frac{f^2}{(1-f)b} \frac{E^2 |\Omega|^2}{4\pi^2} \,. \qquad (3.47)$$

We remark that at this leading-order stability threshold we have $\Phi_0 = \omega$, which then yields $f^2\chi_0^2 = (1-f)b$ and $C_0 = f\chi_0^2 = \frac{1-f}{f} b = -B_0$.

It is critical here to emphasize that the leading order stability threshold is independent of the details of the lattice $\Lambda$, and does not depend on the Bloch vector $\boldsymbol{k}$. In order to determine the effect of the lattice on the stability threshold we must proceed to one higher order.

We now continue the calculation to one higher order. At the leading order stability threshold we can simplify the equation for $\Phi$ and $N$, and we expand the eigenvalue as $\lambda = \nu\lambda_1 + \cdots$ in order to calculate the spectrum

near the origin. At the leading order threshold, the equation for $N_1$ is now

$$\Delta N_1 = \frac{1}{f}\omega^2 - \omega\,, \quad N_1'(0) = 0\,, \quad N_1 \to C_0 \ln|\boldsymbol{y}| + B_1 \quad \text{as} \quad |\boldsymbol{y}| \to \infty\,. \tag{3.48}$$

Upon recalling the definition of $V_{1P}$, it follows that

$$N_1 = \frac{V_{1P}}{f} + B_1\,. \tag{3.49}$$

Since we are seeking the second order term then, as similar to the construction of the equilibrium spot solution, we will need to analyze the third order equation and impose a solvability condition. At the leading order stability threshold, the equation for the third-order term $N_2$ becomes

$$\begin{aligned} &\Delta N_2 + (1 - \frac{2}{f}\omega)\Phi_1 - 3\frac{\omega^2 V_{1P}}{f^3\chi_0^2} - \frac{B_1}{f^2\chi_0^2}\omega^2 - 2\frac{\chi_1}{f\chi_0}\omega^2 = 0\,, \\ &N_2'(0) = 0\,, \quad N_2 \to C_1 \ln|\boldsymbol{y}| + B_2\,, \quad \text{as} \quad |\boldsymbol{y}| \to \infty\,. \end{aligned}$$

The solvability condition for this equation yields that

$$C_1 = -\int_0^\infty \left(1 - \frac{2}{f}\omega\right)\Phi_1 \rho\, d\rho + \frac{3}{f^3\chi_0^2}\int_0^\infty \omega^2 V_{1P}\rho\, d\rho + \frac{B_1}{1-f} + 2\sqrt{\frac{b}{1-f}}\chi_1\,. \tag{3.50}$$

Upon combining this equation with $-2\pi R_{0,\boldsymbol{k}} C_0 - C_1 = B_1$, we derive that

$$\begin{aligned} B_1 = \left(\frac{1-f}{2-f}\right)\Big(&\int_0^\infty (1 - \frac{2}{f}\omega)\Phi_1\rho\, d\rho - \frac{3}{f^3\chi_0^2}\int_0^\infty \omega^2 V_{1P}\rho\, d\rho \\ &+ \frac{2}{f^3\chi_0^2}\int_0^\infty U_{1P}\rho\, d\rho - 2\pi R_{0,\boldsymbol{k}}\frac{1-f}{f}b + 2\sqrt{\frac{b}{1-f}}S_1\Big)\,. \end{aligned} \tag{3.51}$$

Once again, we want to eliminate the term $\int_0^\infty \Phi_1\rho\, d\rho$. This can be done by using the same method as done previously above. To do so, we substitute (3.51) into the equation of $\Phi_1$ to get

$$\mathcal{L}_0\Phi_1 - \lambda_1\omega + \frac{3}{f^2\chi_0^2}\omega^2 V_{1P} + \frac{2\chi_1}{\chi_0}\omega^2 + \frac{B_1}{f\chi_0^2}\omega^2 = 0\,. \tag{3.52}$$

We then integrate both sides of this expression we obtain

$$\int_0^\infty \Phi_1 \rho \, d\rho = \int_0^\infty \Phi_1 \omega \rho \, d\rho - \frac{2-f}{2-2f}\lambda_1 b + \frac{3}{2f^2\chi_0^2}\int_0^\infty \omega^2 V_{1P}\rho \, d\rho + \frac{b\chi_1}{\chi_0} - \pi b R_{0,\boldsymbol{k}} \,. \tag{3.53}$$

Then we substitute (3.53) and (3.51) back into (3.52) to conclude

$$\mathcal{L}\Phi_1 \equiv \mathcal{L}_0\Phi_1 - \frac{\int_0^\infty \Phi_1 \omega \rho \, d\rho}{\int_0^\infty \omega^2 \rho \, d\rho}\omega^2 = \lambda_1\left(\omega + \frac{f}{2-2f}\omega^2\right) - \frac{3}{f^2\chi_0^2}\omega^2 V_{1P} + \left(\frac{3}{2f^2\chi_0^2 b}\int_0^\infty \omega^2 V_{1P}\rho \, d\rho - \frac{\chi_1}{\chi_0} + \pi R_{0,\boldsymbol{k}}\right)\omega^2 \,. \tag{3.54}$$

Finally, $\lambda_1$ is determined by imposing a solvability condition on $\Phi_1$ in (3.54). The adjoint operator of $\mathcal{L}$ is simply

$$\mathcal{L}^\star\Psi \equiv \mathcal{L}_0\Psi - \omega\frac{\int_0^\infty \omega^2\Psi\rho \, d\rho}{\int_0^\infty \omega^2\rho \, d\rho} \,. \tag{3.55}$$

It is readily verified that if we define $\Psi^\star = w + \rho w'/2$, then we have $\mathcal{L}^\star\Psi^* = 0$. The null space of $\mathcal{L}^\star$ was first identified in [8]. By imposing the Fredholm alternative on (3.54) we get

$$\lambda_1\int_0^\infty (\omega + \frac{f}{2-2f}\omega^2)\Psi^*\rho \, d\rho - \frac{3}{2f^2\chi_0^2}\int_0^\infty \omega^2 V_{1P}\Psi^*\rho \, d\rho + (\frac{3}{2f^2\chi_0^2 b}\int_0^\infty \omega^2 V_{1P}\rho \, d\rho - \frac{\chi_1}{\chi_0} + \pi R_{0,\boldsymbol{k}})\int_0^\infty \omega^2\Psi^*\rho \, d\rho = 0 \,. \tag{3.56}$$

This expression can be simplified considerably by using the following identities:

$$\int_0^\infty \omega^2\Psi^*\rho \, d\rho = \int_0^\infty (L_0\omega)\left(L_0^{-1}\omega\right) = \int_0^\infty \omega^2\rho \, d\rho = b \,,$$
$$\int_0^\infty \omega\Psi^*\rho \, d\rho = \int_0^\infty \rho\omega(\omega + \frac{\rho}{2}\omega') \, d\rho = \int_0^\infty \omega^2\rho \, d\rho + \frac{1}{4}\int_0^\infty \left[\omega^2\right]'\rho^2 \, d\rho = \frac{b}{2} \,,$$
$$\int_0^\infty \omega^2 V_{1P}\Psi^*\rho \, d\rho = \int_0^\infty (L_0U_{1P})\left(L_0^{-1}\omega\right) = \int_0^\infty U_{1P}\omega\rho \, d\rho \,,$$

$$2\int_0^\infty \omega U_{1P}\Psi^*\rho\,d\rho - \int_0^\infty U_{1P}\rho\,d\rho = \int_0^\infty \omega^2 V_{1P}\rho\,d\rho\,.$$

In this way, we determine the spectrum near the origin in the spectral plane as

$$\lambda_1 = 2(1-f)\left(\frac{\chi_1}{\chi_0} - \pi R_{0,\boldsymbol{k}} + \frac{3}{2f^2\chi_0^2 b}\int_0^\infty U_{1P}\rho\,d\rho\right). \tag{3.57}$$

Since we are seeking a two-term expansion for the stability threshold $D_c$ of $D$, we need to write $\chi_0$ and $\chi_1$ in term of $D$. In Principal Result 1, $\chi$ was written in term of $S$, and $S$ is in term of $D$ as

$$\begin{aligned} S &= \nu^{\frac{1}{2}}(S_0 + \nu S_1 + \cdots) = \frac{E|\Omega|}{2\pi\sqrt{D}} = \frac{E|\Omega|}{2\pi}\left[D_0\left(1+\nu\frac{D_1}{D_0}+\cdots\right)\right]^{-\frac{1}{2}} \\ &= \nu^{-\frac{1}{2}}\frac{E|\Omega|D_0^{-\frac{1}{2}}}{2\pi}\left(1-\frac{\nu}{2}\frac{D_1}{D_0}+\cdots\right). \end{aligned}$$

Now with $D_{c0} = \frac{f^2}{(1-f)b}\frac{E^2|\Omega|^2}{4\pi^2}$, we have $S_{c1} = -\frac{1}{2}S_0\frac{D_{c1}}{D_{c0}}$, so that

$$\frac{\chi_1}{\chi_0} = \frac{f\chi_0}{b}\left(-\frac{1}{f^3\chi_0^3}\int_0^\infty U_{1P}\rho\,d\rho - S_1\frac{f}{1-f}\right).$$

Therefore, we have

$$\lambda_1 = 2(1-f)\left(\frac{1}{2(1-f)b^2}\int_0^\infty U_{1P}\rho\,d\rho + \frac{2\pi^2(1-f)b}{f^2E^2|\Omega|^2}D_1 - \pi R_{0,\boldsymbol{k}}\right). \tag{3.58}$$

Notice that this is a continuous band of spectra parametrized by the Bloch vector $\boldsymbol{k}$. This is illustrated schematically in Figure 3.2. As proved in Lemma 1 and Lemma 2, $R_{0,\boldsymbol{k}}$ is real and tends to infinity as $|\boldsymbol{k}| \to 0$. This shows from (3.58) that $\lambda_1$ is real, and leaves the ball of radius $\mathcal{O}(\nu) \ll 1$ near the origin along the negative real axis as $|\boldsymbol{k}| \to 0$.

Therefore, in order to have stability, we need $\lambda_1 < 0$, $\forall \boldsymbol{k} \in \Omega^*$. We summarize our result as follows:

**Principal Result 2.** *In the limit $\epsilon \to 0$, $D \sim \mathcal{O}(\frac{1}{\nu})$, we have constructed*

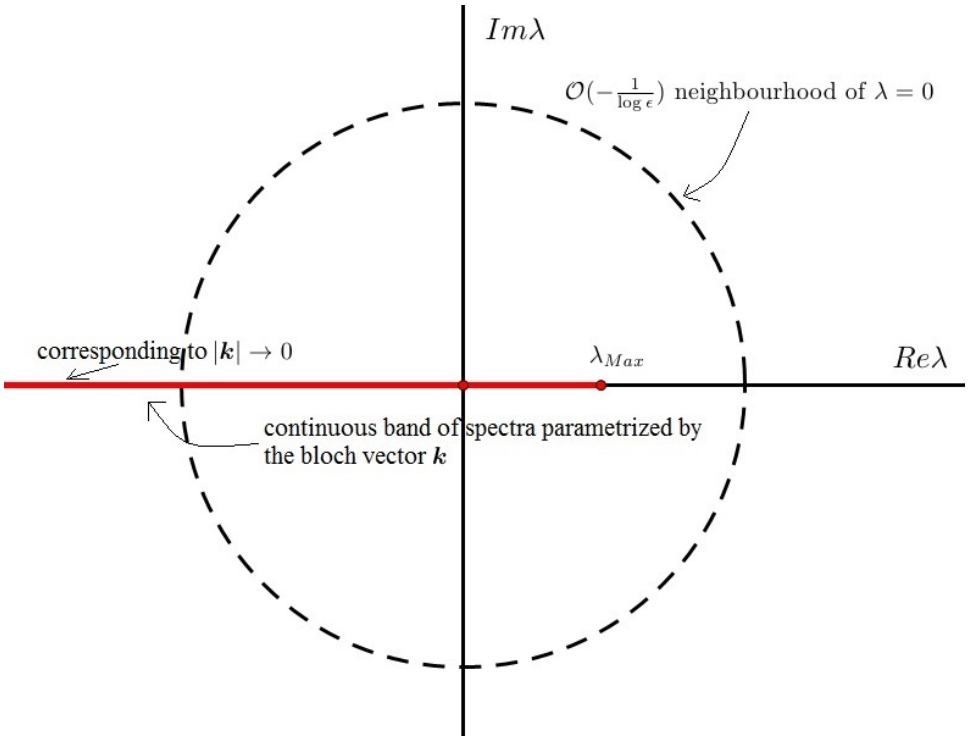


Figure 3.1: The Continuous Band of Spectra

*periodic spot solutions(with respect to a fixed Bravais lattice $\Lambda$) in Principal Result 1. The linearized operator around this solution has a continuous spectrum within an $\mathcal{O}(\nu)$ neighbourhood of the origin and is parametrized by a Bloch vector $\boldsymbol{k} \in \Omega^* \backslash \mathbf{0}$:*

$$\lambda(\boldsymbol{k}) = 2\nu(1-f)\left(\frac{1}{2(1-f)b^2}\int_0^\infty U_{1P}\rho\, d\rho + \frac{2\pi^2(1-f)b}{f^2E^2|\Omega|^2}D_1 - \pi R_{0,\boldsymbol{k}}\right). \tag{3.59}$$

*To have linear stability, we need $\lambda(\boldsymbol{k}) < 0$, $\forall \boldsymbol{k} \in \Omega^* \backslash \mathbf{0}$, which gives a two term asymptotic expansion for the stability threshold $D_c$:*

$$D_c = \frac{D_{c0}}{\nu} + D_{c1} + \cdots, \quad \textit{where} \quad D_{c0} = \frac{f^2E^2|\Omega|^2}{4\pi^2(1-f)b}, \quad \textit{and}$$
$$D_{c1} = \min_{\boldsymbol{k}\in\Omega^*\backslash\mathbf{0}}\{\frac{f^2E^2|\Omega|^2}{2\pi^2(1-f)b}(\pi R_{0,\boldsymbol{k}} - \frac{1}{2(1-f)b^2}\int_0^\infty U_{1P}\rho\, d\rho)\},$$

$$= \min_{\boldsymbol{k}\in\Omega^*\setminus\mathbf{0}} \{D_{c0}(2\pi R_{0,\boldsymbol{k}} - \frac{1}{(1-f)b^2}\int_0^\infty U_{1P}\rho\, d\rho)\}$$
$$= \min_{\boldsymbol{k}\in\Omega^*\setminus\mathbf{0}} \{D_{c0}(2\pi R_{0,\boldsymbol{k}} + \frac{1}{(1-f)b^2}\int_0^\infty U_{1QI}\rho\, d\rho - \frac{1}{b^2}\int_0^\infty U_{1QII}\rho\, d\rho)\}\,.$$

We remark here that since $R_{0,\boldsymbol{k}}$ is real-valued, then so is the threshold $D_c$, which is what we should expect. As shown above, the second order term in $D_c$ depends on the lattice $\Lambda$. In order to compare the stability threshold on different lattices, we will fix $|\Omega| = 1$. This leads to the following optimality criterion:

**Principal Result 3.** *With fixed primitive cell of area unity, the optimal lattice arrangement $\Lambda_{op}$ is the one with the largest stability threshold:*

$$\Lambda_{op} = \arg\max_{\Lambda,\ |\Omega|=1}\{D_c(\Lambda)\} = \arg\max_{\Lambda,\ |\Omega|=1}\{\min_{\boldsymbol{k}\in\Omega^*\setminus\mathbf{0}}\{R_{0,\boldsymbol{k}}\}\}\,. \tag{3.60}$$

Some numerical results to identify the optimal lattice arrangement is given in Section 5.2.

## 3.3 A Quick Derivation of the Stability Threshold

In this section, we give another much more expedient way to derive the stability threshold. Recall that in the inner core problem (3.3), $S$ is a parameter in the asymptotic boundary condition. More specifically, if we view $S$ as a parameter of the solution, then

$$\begin{aligned}
&\Delta_\rho U(|\boldsymbol{y}|,S) - U(|\boldsymbol{y}|,S) + fU^2(|\boldsymbol{y}|,S)V(|\boldsymbol{y}|,S) = 0\,,\\
&\frac{\partial U}{\partial\rho}(0,S) = 0\,, \quad U\to 0 \quad \text{as} \quad |\boldsymbol{y}|\to\infty\,,\\
&\Delta_\rho V(|\boldsymbol{y}|,S) + U(|\boldsymbol{y}|,S) - U^2(|\boldsymbol{y}|,S)V(|\boldsymbol{y}|,S) = 0\,,\\
&\frac{\partial V}{\partial\rho}(0,S) = 0\,, \quad V\to S\ln|\boldsymbol{y}| + \chi(S,f) \quad \text{as} \quad |\boldsymbol{y}|\to\infty\,.
\end{aligned}$$

Upon taking the partial derivative of $U$ and $V$ with respect to $S$, we get

$$\Delta \begin{pmatrix} \frac{\partial U}{\partial S} \\ \frac{\partial V}{\partial S} \end{pmatrix} + \begin{pmatrix} -1+2fUV & fU^2 \\ 1-2UV & -U^2 \end{pmatrix} \begin{pmatrix} \frac{\partial U}{\partial S} \\ \frac{\partial V}{\partial S} \end{pmatrix} = \begin{pmatrix} 0 \\ 0 \end{pmatrix}, \tag{3.61}$$

with the boundary conditions

$$\begin{aligned} &\frac{\partial^2 U}{\partial S \partial \rho}(0,S) = 0\,, \quad \frac{\partial U}{\partial S} \to 0\,, \quad \text{as} \quad |\boldsymbol{y}| \to \infty\,, \\ &\frac{\partial^2 V}{\partial S \partial \rho}(0,S) = 0\,, \quad \frac{\partial V}{\partial S} \to \ln|\boldsymbol{y}| + \frac{\partial \chi}{\partial S}(S,f)\,, \quad \text{as} \quad |\boldsymbol{y}| \to \infty\,. \end{aligned}$$

Then, we observe that $\frac{\partial U}{\partial S}$ and $\frac{\partial V}{\partial S}$ are, up to a scalar multiple, the solution to the perturbed core problem (3.33) and (3.34) when $\lambda = 0$. To fix the boundary conditions in (3.33) and (3.34) for $N(\boldsymbol{y})$, we must choose $S$ appropriately. This constraint on $S$ to hold when $\lambda = 0$ is the stability threshold we are seeking. Since the solution to (3.33) and (3.34) is unique up to a constant scaling, then upon comparing the boundary conditions with (3.33) and (3.34), it follows that the stability threshold $S_c$ occurs when

$$\frac{B}{C} = \frac{\partial \chi}{\partial S}(S_c, f)\,. \tag{3.62}$$

Then, together with (3.40), we have

$$\frac{\partial}{\partial S}\chi(S_c, f) = -\frac{1}{\nu} - 2\pi R_{0,\boldsymbol{k}} + \mathcal{O}(\nu)\,. \tag{3.63}$$

We then use the expansion for $\chi$ from Principal Result 1, which we write as

$$\begin{aligned} &\chi(S,f) = \nu^{-\frac{1}{2}} \left( \frac{b(1-f)}{f^2}\frac{1}{S_0} + \nu(-\frac{(1-f)b}{f^2}\frac{S_1}{S_0^2} - \frac{S_0}{(1-f)b^2}\int_0^\infty U_{1P}\rho\, d\rho) + \cdots \right), \\ &S = \nu^{\frac{1}{2}}(S_0 + \nu S_1 + \cdots)\,, \end{aligned}$$

to derive

$$\chi(S,f) = \frac{b(1-f)}{f^2}\frac{1}{S} - \frac{\int_0^\infty U_{1P}\rho\, d\rho}{(1-f)b^2}S + \mathcal{O}(\nu)\,, \tag{3.64}$$

$$= \frac{b(1-f)}{f^2}\frac{1}{S} + \left(\frac{1}{b^2(1-f)}\int_0^\infty U_{1QI}\rho\,d\rho - \frac{1}{b^2}\int_0^\infty U_{1QII}\rho\,d\rho\right)S + \mathcal{O}(\nu)\,.$$

Upon taking the partial derivative we obtain

$$\begin{aligned}\frac{\partial}{\partial S}\chi(S,f) &= -\frac{b(1-f)}{f^2}\frac{1}{S^2} - \frac{\int_0^\infty U_{1P}\rho\,d\rho}{(1-f)b^2} + \mathcal{O}(\nu)\,, \qquad (3.65)\\ &= -\frac{1}{\nu}\frac{b(1-f)}{f^2}\frac{1}{S_0^2}(1 - 2\frac{S_1}{S_0}\nu + \cdots) - \frac{\int_0^\infty U_{1P}\rho\,d\rho}{(1-f)b^2} + \mathcal{O}(\nu)\,,\\ &= -\frac{1}{\nu}\frac{b(1-f)}{f^2}\frac{1}{S_0^2} + (2\frac{b(1-f)}{f^2}\frac{S_1}{S_0^3} - \frac{\int_0^\infty U_{1P}\rho\,d\rho}{(1-f)b^2}) + \mathcal{O}(\nu)\,.\end{aligned}$$

Upon comparing this expression with (3.63), we obtain from equating powers of $\nu$ that

$$\begin{aligned}-1 &= -\frac{b(1-f)}{f^2}\frac{1}{S_{c0}^2}\,,\\ -2\pi R_{0,\boldsymbol{k}} &= 2\frac{b(1-f)}{f^2}\frac{S_{c1}}{S_{c0}^3} - \frac{\int_0^\infty U_{1P}\rho\,d\rho}{(1-f)b^2}\,,\\ &= 2\frac{b(1-f)}{f^2}\frac{S_{c1}}{S_{c0}^3} + \frac{1}{b^2(1-f)}\int_0^\infty U_{1QI}\rho\,d\rho - \frac{1}{b^2}\int_0^\infty U_{1QII}\rho\,d\rho\,.\end{aligned}$$

In this way, we can solve for $S_{c0}$ and $S_{c1}$, then obtain the corrections $D_{c0}$ and $D_{c1}$ to the stability threshold from expanding the relation (3.8) between $S$ and $D$. This yields the same result for the stability threshold as derived in Principal Result 2. We remark that although this simple derivation is able to quickly isolate the stability threshold, it is unable to give any precise account of the nature of the spectrum of the linearized operator near the origin when $D$ is near the leading-order stability threshold.

# Chapter 4

# Spot Patterns for the Brusselator on a Finite Domain

In this chapter, we first construct $N$-spot solutions to the Brusselator model, formulated as

$$\begin{aligned} u_t &= \epsilon^2 \Delta u - u + f(u^2 v + 2\epsilon^2 E u v + \epsilon^4 E v)\,, \\ \tau v_t &= D\Delta v + E + \epsilon^{-2}(u - u^2 v) - 2Euv - \epsilon^2 E^2 v\,, \end{aligned} \tag{4.1}$$

on a finite domain $\boldsymbol{x} \in \Omega \subset \mathbf{R}^2$, with no-flux boundary conditions

$$\partial_{\boldsymbol{n}} u(\boldsymbol{x}) = \partial_{\boldsymbol{n}} v(\boldsymbol{x}) = 0\,, \qquad \boldsymbol{x} \in \partial\Omega\,, \tag{4.2}$$

where $\boldsymbol{n}$ is the outer normal vector on $\partial\Omega$. After constructing such multi-spot patterns, we then perform a linear stability analysis to calculate a stability threshold corresponding to a zero-eigenvalue crossing.

The asymptotic construction of the $N$-spot pattern and the linear stability analysis is very similar to that for the periodic case. One of the key differences between the periodic and finite-domain problems, is that for the periodic case we need only construct a one-spot solution in one primitive cell. In contrast, for the finite domain case, spots interact with each other in the domain through the Green's function. As a result, a Neumann Green matrix together with its eigenvalues and eigenvectors play a key role in the analysis.

## 4.1 The $N$-Spot Solutions

In this section, our goal is to construct $N$-spot solutions where $u(\boldsymbol{x})$ concentrates around $N$ distinct $\mathcal{O}(\epsilon)$ balls centred at $N$ given points $\boldsymbol{x}_1, \boldsymbol{x}_2, ..., \boldsymbol{x}_n \in \Omega$. The position of these $N$ points are not arbitrary, but satisfy some conditions to be derived and explained below.

We first introduce local coordinates around each of these $N$ points in the form

$$\boldsymbol{y} = \epsilon^{-1}(\boldsymbol{x} - \boldsymbol{x}_j)\,, \quad U_j(\boldsymbol{y}) = \frac{u(\boldsymbol{x})}{\sqrt{D}}\,, \quad V_j(\boldsymbol{y}) = \sqrt{D}v(\boldsymbol{x})\,, \quad j = 1, 2, ..., N\,. \tag{4.3}$$

Then, in an inner region around $\boldsymbol{x}_j$, we look for a radially symmetric solution in the form $U_j(\boldsymbol{y}) = U_j(\rho),\ V_j(\boldsymbol{y}) = V_j(\rho)$, where $\rho = |\boldsymbol{y}|$. To leading order, we get the core problem

$$\Delta_\rho U_j - U_j + fU_j^2 V_j = 0\,, \quad \Delta_\rho V_j + U_j - U_j^2 V_j = 0\,, \quad 0 < \rho < \infty\,, \tag{4.4}$$

with the boundary conditions

$$U_j'(0) = V_j'(0) = 0\,, \quad U_j \to 0\,, \quad V_j \to S_j \ln\rho + \chi(S_j, f)\,, \quad \text{as} \quad \rho \to \infty\,. \tag{4.5}$$

Here the introduction of the source strength $S_j$ and the function $\chi(S_j, f)$ is the same as in (3.4). Upon integrating $\Delta V_j$ and using the divergence theorem we get

$$2\pi S_j = \int_{\mathbf{R}^2} (U_j^2 V_j - U_j)\, d\boldsymbol{x} = \int_0^{2\pi} d\theta \int_0^\infty (U_j^2 V_j - U_j)\rho\, d\rho\,,$$

which yields

$$S_j = \int_0^\infty (U_j^2 V_j - U_j)\rho\, d\rho\,. \tag{4.6}$$

In the outer region, given that $u$ is localized around $\{\boldsymbol{x}_i\}_{i=1}^N$, then by using the relation (4.6) we obtain that the leading order outer solution $v$

satisfies

$$D\Delta v + E = 2\pi\sqrt{D}\sum_{i=1}^{N} S_i\delta(\boldsymbol{x}-\boldsymbol{x_i})\,, \qquad \boldsymbol{x}\in\Omega\,, \tag{4.7}$$

with $\partial_{\boldsymbol{n}} v = 0$ for $\boldsymbol{x}\in\partial\Omega$. Upon integrating (4.7) over $\Omega$, and by using the no-flux boundary conditions (4.2), we get the solvability condition

$$E = \frac{2\pi\sqrt{D}}{|\Omega|}\sum_{j=1}^{N} S_j\,. \tag{4.8}$$

To represent the solution $v$, it is convenient to introduce the Neumann Green function $G(\boldsymbol{x},\boldsymbol{\xi})$, which satisfies

$$\Delta_{\boldsymbol{x}} G_0(\boldsymbol{x},\boldsymbol{\xi}) = \frac{1}{|\Omega|} - \delta(\boldsymbol{x}-\boldsymbol{\xi})\,, \tag{4.9}$$

$$\nabla_{\boldsymbol{x}} G_0(\boldsymbol{x},\boldsymbol{\xi})\cdot\boldsymbol{n} = 0\,, \quad \forall\boldsymbol{x}\in\partial\Omega\,, \quad \int_\Omega G_0(\boldsymbol{x},\boldsymbol{\xi})\,d\boldsymbol{x} = 0\,, \tag{4.10}$$

$$G_0(\boldsymbol{x},\boldsymbol{\xi}) \to -\frac{1}{2\pi}\ln|\boldsymbol{x}-\boldsymbol{\xi}| + R_0(\boldsymbol{\xi})\,, \quad \text{as} \quad \boldsymbol{x}\to\boldsymbol{\xi}\,, \tag{4.11}$$

where $\boldsymbol{n}$ is the outer normal vector to $\partial\Omega$. We remark here that $R(\boldsymbol{\xi})$ is the regular part of the Green function while $-\frac{1}{2\pi}\ln|\boldsymbol{x}-\boldsymbol{\xi}|$ is the singular part. The right hand side of the equation $\frac{1}{|\Omega|} - \delta(\boldsymbol{x}-\boldsymbol{\xi})$ is consistent with the no-flux boundary conditions $\nabla_{\boldsymbol{x}} G_0(\boldsymbol{x},\boldsymbol{\xi})\cdot\boldsymbol{n} = 0,\ \forall\boldsymbol{x}\in\partial\Omega$. We also impose the uniqueness condition, $\int_\Omega G_0(\boldsymbol{x},\boldsymbol{\xi})\,d\boldsymbol{x} = 0$, since the solution to the PDE with the no-flux boundary conditions is only unique up to a constant.

In terms of $G_0$, the solution $v$ to (4.7) can be represented as

$$v(\boldsymbol{x}) = -\sum_{i=1}^{N}\frac{2\pi S_i}{\sqrt{D}}G_0(\boldsymbol{x},\boldsymbol{x}_i) + c\,, \tag{4.12}$$

where $c$ is some constant. Then, by letting $\boldsymbol{x}\to\boldsymbol{x}_j$, and by matching to the inner solution near each spot, we obtain the following nonlinear system of

$N$ equations for $S_j$, $j = 1, \ldots, N$, and for $c$:

$$\frac{S_j}{\nu} + \chi(S_j) = -2\pi R_0(\boldsymbol{x}_j)S_j - 2\pi \sum_{i \neq j} G_0(\boldsymbol{x}_i, \boldsymbol{x}_j)S_i + \sqrt{D}c\,, \quad 1 \leq j \leq N\,. \tag{4.13}$$

The remaining equation to complete the system is (4.8). It is convenient to rewrite this system in matrix form by introducing the following notation:

$$\boldsymbol{S} \equiv \begin{pmatrix} S_1 \\ \vdots \\ S_N \end{pmatrix}\,, \quad \boldsymbol{e} \equiv \begin{pmatrix} 1 \\ \vdots \\ 1 \end{pmatrix}\,, \quad \chi(\boldsymbol{S}, f) \equiv \begin{pmatrix} \chi(S_1, f) \\ \vdots \\ \chi(S_N, f) \end{pmatrix}\,,$$

$$\mathcal{G} \equiv \begin{pmatrix} R_0(\boldsymbol{x}_1) & G_0(\boldsymbol{x}_1, \boldsymbol{x}_2) & \cdots & G_0(\boldsymbol{x}_1, \boldsymbol{x}_N) \\ G_0(\boldsymbol{x}_2, \boldsymbol{x}_1) & R_0(\boldsymbol{x}_2) & \cdots & \\ \vdots & \ddots & & \vdots \\ G_0(\boldsymbol{x}_N, \boldsymbol{x}_1) & \cdots & & R_0(\boldsymbol{x}_N) \end{pmatrix}\,.$$

We shall refer to $\mathcal{G}$ as the Neumann Green matrix of $\boldsymbol{x}_1, \boldsymbol{x}_2, ..., \boldsymbol{x}_N$. Then, the $N$ matching conditions (4.13) and the solvability condition (4.8) can be written in matrix form as

$$\begin{aligned} &\boldsymbol{S} + \nu\chi(\boldsymbol{S}, f) = -\nu 2\pi \mathcal{G}\boldsymbol{S} + \nu\sqrt{D}c\boldsymbol{e}\,, \\ &\boldsymbol{e}^T\boldsymbol{S} = \frac{|\Omega|E}{2\pi\sqrt{D}}\,. \end{aligned} \tag{4.14}$$

For simplicity we will assume that the $N$ spots have a common source strength $S$, i.e. for $S_j = S,\ j = 1, 2, ..., N$. For such a pattern, we have that $\boldsymbol{S} = S\boldsymbol{e}$, $\chi(\boldsymbol{S}, f) = \chi(S, f)\boldsymbol{e}$, and that (4.14) reduces to

$$\mathcal{G}\boldsymbol{S} = S\mathcal{G}\boldsymbol{e} = -\frac{1}{2\pi\nu}(S + \nu\chi(S, f) - \nu\sqrt{D}c)\boldsymbol{e}\,, \qquad S = \frac{E|\Omega|}{2\pi N\sqrt{D}}\,. \tag{4.15}$$

Therefore, it follows that for such a common source strength pattern to exist we must have that $\boldsymbol{e}$ is an eigenvector of $\mathcal{G}(\boldsymbol{x}_1, \boldsymbol{x}_2, ..., \boldsymbol{x}_N)$. We remark that the existence of such a special eigenvalue does not generally occur for a pattern of $N$ arbitrarily-located spots. Since the Green function satisfies

the usual reciprocity condition, it follows that $\mathcal{G}$ is a symmetric matrix and can be diagonalized with an orthonormal basis as $\frac{1}{\sqrt{N}}\boldsymbol{e}$, $\{\boldsymbol{q}_j\}_{j=2}^N$, i.e.

$$\mathcal{G}(\frac{1}{\sqrt{N}}\boldsymbol{e}) = k_1(\frac{1}{\sqrt{N}}\boldsymbol{e})\,, \quad \mathcal{G}\boldsymbol{q}_j = k_j\boldsymbol{q}_j\,, \quad j = 2,3,...,N, \tag{4.16}$$
$$\boldsymbol{q}_j^T\frac{1}{\sqrt{N}}\boldsymbol{e} = 0\,, \quad j = 2,3,...,N\,, \quad \boldsymbol{q}_j^T\boldsymbol{q}_i = 0\,, \quad \forall\ 2 \le i,j \le N\,.$$

Upon using this relation, we obtain for a common source strength pattern that (4.14) reduces to

$$\frac{1}{2\pi\nu}(S + \nu\chi(S,f) - \nu\sqrt{D}c) = -Sk_1\,. \tag{4.17}$$

Next, since the stability threshold occurs in the regime where $D \sim \mathcal{O}(\nu^{-1})$, it follows that $S \sim \mathcal{O}(\nu^{\frac{1}{2}})$ at a zero eigenvalue crossing. By following the same procedure as for the periodic problem, we can calculate the small $S$ asymptotics of the solution to the core problem (4.4) as follows:

**Principal Result 4.** *For $S \sim \nu^{\frac{1}{2}}(S_0 + \nu S_1 + \cdots)$, where $\nu \equiv -\frac{1}{\ln\epsilon}$, the radially symmetric asymptotic solutions to the core problem (4.4) in an $\mathcal{O}(\epsilon)$ ball centred at $\boldsymbol{x}_j$ is given by:*

$$U_j \sim \nu^{\frac{1}{2}}(U_{j0} + \nu U_{j1} + \cdots)\,, \quad V_j \sim \nu^{-\frac{1}{2}}(V_{j0} + \nu V_{j1} + \cdots)\,,$$
$$\chi \sim \nu^{-\frac{1}{2}}(\chi_0 + \nu\chi_1 + \cdots)\,, \tag{4.18}$$

*where $U_{j0}(\rho)$, $U_{j1}(\rho)$, $V_{j0}(\rho)$ and $V_{j1}(\rho)$ are defined by*

$$U_{j0} = \frac{\omega}{f\chi_0}\,, \qquad U_{j1} = -\frac{\chi_1}{f\chi_0^2}\omega - \frac{1}{f^3\chi_0^3}((1-f)U_{1QII} - U_{1QI})\,, \tag{4.19}$$
$$V_{j0} = \chi_0\,, \qquad V_{j1} = \chi_1 + \frac{1}{f^2\chi_0}((1-f)V_{1Q} - \omega)\,. \tag{4.20}$$

*Here $U_{1QI}$, $U_{1QII}$, $V_{1Q}$ are the unique radially symmetric solutions to (3.26), (3.26), (3.24) as before, $\omega$ is the unique radially symmetric solution to*

*(3.17), while* $\chi_0$ *and* $\chi_1$ *are defined as*

$$\chi_0 = \frac{(1-f)}{f^2}\frac{b}{S_0}\,, \tag{4.21}$$

$$\chi_1 = -\frac{(1-f)b}{f^2}\frac{S_1}{S_0^2} - \frac{S_0}{b^2}\int_0^\infty U_{1QII}\rho\,d\rho + \frac{S_0}{(1-f)b^2}\int_0^\infty U_{1QI}\rho\,d\rho\,. \tag{4.22}$$

We remark here that since the source strength is the same for each $j$, then so are the inner solutions. Moreover, we remark that such patterns can either be true steady-state solutions if the spot locations satisfy some further condition, or simply quasi-steady patterns that can persist for very long time intervals provided that there is no unstable $\mathcal{O}(1)$ eigenvalue in the spectrum of the linearization. The analysis of the spectrum of the linearization is analyzed in the next section. This completes our construction of an $N$-spot solution where the spots have a common source strength.

## 4.2 Linear Stability Analysis

We denote the $N$-spot solution constructed above as $u_e(\boldsymbol{x})$, $v_e(\boldsymbol{x})$ and we introduce the perturbation

$$u(\boldsymbol{x}) = u_e(\boldsymbol{x}) + e^{\lambda t}\phi\,, \qquad v(\boldsymbol{x}) = v_e(\boldsymbol{x}) + e^{\lambda t}\eta\,. \tag{4.23}$$

Upon substituting (4.23) into (4.1), we linearize around the $N$-spot solution to obtain the singularly perturbed problem (3.31), written again as

$$\lambda\begin{pmatrix}\phi\\ \tau\eta\end{pmatrix} = \begin{pmatrix}\epsilon^2\Delta\phi\\ D\Delta\eta\end{pmatrix} + \begin{pmatrix}-1+2fu_ev_e & fu_e^2\\ \epsilon^{-2}-2\epsilon^{-2}u_ev_e & \epsilon^{-2}u_e^2\end{pmatrix}\begin{pmatrix}\phi\\ \eta\end{pmatrix}.$$

In the inner region around each $\boldsymbol{x}_j$, we introduce the local variables as

$$\boldsymbol{y} = \epsilon^{-1}(\boldsymbol{x}-\boldsymbol{x}_j)\,, \quad \Phi_j(\boldsymbol{y}) = \frac{\phi(\epsilon\boldsymbol{y}+\boldsymbol{x}_j)}{D}\,, \quad N_j(\boldsymbol{y}) = \eta(\epsilon\boldsymbol{y}+\boldsymbol{x}_j)\,. \tag{4.24}$$

We look for radially symmetric solution of the form $\Phi_j(\boldsymbol{y}) = \Phi_j(\rho)$, $N_j(\boldsymbol{y}) =$

$N_j(\rho)$, where $\rho = |\boldsymbol{y}|$. Then, the inner problem near the $j$-th spot at $\boldsymbol{x}_j$ reduces asymptotically to

$$\begin{aligned}
&\Delta_\rho \Phi_j - (\lambda+1)\Phi_j + 2fU_jV_j\Phi + fU_j^2 N_j = 0\,, \qquad (4.25)\\
&\Delta_\rho N_j + (1-2U_jV_j)\Phi_j - U_j^2 N_j = 0\,,\\
&\Phi_j'(0) = N_j'(0) = 0\,; \quad \Phi_j \to 0\,, \quad N_j \to C_j \ln|\boldsymbol{y}| + B_j(C_j, f)\,, \quad \text{as} \quad \rho \to \infty\,.
\end{aligned}$$

We remark here that for a fixed $f$, the ratio $\frac{B_j}{C_j}$ is a constant since the system is linear. The solvability condition for the $N_j$ equation yields

$$C_j = \int_0^\infty \left(U_j^2 N_j - (1-2U_jV_j)\Phi_j\right)\rho\, d\rho\,. \qquad (4.26)$$

Since both $u_e(\boldsymbol{x})$ and $\phi(\boldsymbol{x})$ are localized near $\{\boldsymbol{x}_j\}_{j=1}^N$, the outer approximation for the eigenfunction component $\eta(\boldsymbol{x})$ satisfies the leading order problem

$$\Delta\eta - \frac{\tau\lambda}{D}\eta = 2\pi \sum_{i=1}^N C_i \delta(\boldsymbol{x} - \boldsymbol{x}_i)\,. \qquad (4.27)$$

Notice that when $\lambda = 0$, corresponding to the stability threshold, then if we integrate (4.27) over the domain and use the no-flux boundary condition we conclude that $\sum_{j=1}^N C_j = 0$. However, we do not have this constraint when $\lambda \neq 0$. This observation suggest that we need to split our analysis into several cases.

### 4.2.1 $\lambda \neq 0$ and $\lambda \sim \mathcal{O}(1)$

First we introduce the reduced-wave Green function, which satisfies

$$\begin{aligned}
&\Delta_{\boldsymbol{x}} G_\sigma(\boldsymbol{x}, \boldsymbol{\xi}) - \sigma^2 G_\sigma(\boldsymbol{x}, \boldsymbol{\xi}) = -\delta(\boldsymbol{x} - \boldsymbol{\xi})\,, \qquad (4.28)\\
&\nabla_{\boldsymbol{x}} G_\sigma(\boldsymbol{x}, \boldsymbol{\xi}) \cdot \boldsymbol{n} = 0\,, \quad \forall \boldsymbol{x} \in \partial\Omega\,, \qquad (4.29)\\
&G_\sigma(\boldsymbol{x}, \boldsymbol{\xi}) \to -\frac{1}{2\pi}\ln|\boldsymbol{x} - \boldsymbol{\xi}| + R_\sigma(\boldsymbol{\xi})\,, \quad \text{as} \quad \boldsymbol{x} \to \boldsymbol{\xi}\,. \qquad (4.30)
\end{aligned}$$

We need an approximation to this Green's function when $\sigma \ll 1$. Since there is no solution when $\sigma = 0$, then as we did in (2.3) we must seek $G_\sigma$

for $\sigma \ll 1$ in the form of a singular asymptotic expansion as

$$G_\sigma(\boldsymbol{x}, \boldsymbol{\xi}) = \frac{1}{\sigma^2 |\Omega|} + G_0(\boldsymbol{x}, \boldsymbol{\xi}) + \mathcal{O}(\sigma^2)\,, \tag{4.31}$$

where $G_0(\boldsymbol{x}, \boldsymbol{\xi})$ is the Neumann Green function defined in (4.9). Then if we denote $\sigma = \frac{\tau\lambda}{D}$, we can represent the solution to (4.27) in the form

$$\eta(\boldsymbol{x}) = -2\pi \sum_{i=1}^{N} C_i G_\sigma(\boldsymbol{x}, \boldsymbol{x}_i) = 2\pi \sum_{i=1}^{N} C_i \left( -\frac{D}{\tau\lambda|\Omega|} - G_0(\boldsymbol{x}, \boldsymbol{x}_i) + \mathcal{O}(\sigma^2) \right). \tag{4.32}$$

By expanding this solution as $\boldsymbol{x} \to \boldsymbol{x}_j$ and comparing the resulting expression with the far-field behavior of the corresponding inner solution, we obtain the following matching condition near each spot:

$$\frac{C_j}{\nu} + B_j = -\frac{2\pi D}{\tau\lambda|\Omega|} \sum_{i=1}^{N} C_i - 2\pi R(\boldsymbol{x}_j) C_j - \sum_{i \neq j} 2\pi G_0(\boldsymbol{x}_i, \boldsymbol{x}_j) C_i\,, \quad 1 \leq j \leq N\,. \tag{4.33}$$

We then rewrite this system in matrix form by first introducing the notation

$$\boldsymbol{C} \equiv \begin{pmatrix} C_1 \\ \vdots \\ C_N \end{pmatrix}, \quad \boldsymbol{B} \equiv \begin{pmatrix} B_1 \\ \vdots \\ B_N \end{pmatrix}, \quad \boldsymbol{\Phi} \equiv \begin{pmatrix} \Phi_1 \\ \vdots \\ \Phi_N \end{pmatrix}, \quad \boldsymbol{N} \equiv \begin{pmatrix} N_1 \\ \vdots \\ N_N \end{pmatrix}, \tag{4.34}$$

$$\mathcal{E} \equiv \frac{1}{N} \boldsymbol{e}\boldsymbol{e}^T = \frac{1}{N} \begin{pmatrix} 1 & 1 & \cdots & 1 \\ \vdots & \ddots & & \vdots \\ 1 & \cdots & & 1 \end{pmatrix}. \tag{4.35}$$

In terms of these new variables, (4.33) can be written in matrix form as

$$\left( I + \frac{2\pi\nu DN}{\tau\lambda|\Omega|} \mathcal{E} + 2\pi\nu \mathcal{G} \right) \boldsymbol{C} = -\nu \boldsymbol{B}\,. \tag{4.36}$$

From this system it follows that $\boldsymbol{B}$ is one order higher in $\nu$ than $\boldsymbol{C}$ when $\lambda \sim \mathcal{O}(1)$. Moreover, since the system (4.4) is linear, we may assume

$N(\boldsymbol{y}) \sim \mathcal{O}(1)$. This suggests that we introduce the asymptotic expansion as

$$\Phi_j \sim \nu(\Phi_{j0} + \nu\Phi_{j1} + \cdots)\,, \qquad N_j \sim N_{j0} + \nu N_{j1} + \cdots\,, \tag{4.37}$$
$$B_j \sim B_{j0} + \nu B_{j1} + \cdots\,, \qquad C_j \sim \nu(C_{j0} + \nu C_{j1} + \cdots)\,.$$

Upon substituting this expansion into (4.25), and by using the results from Principal Result 4, we obtain at leading order that

$$\Delta_\rho \Phi_{j0} - (\lambda+1)\Phi_{j0} + 2fU_{j0}V_{j0}\Phi_{j0} + fU_{j0}^2 N_{j0} = 0\,, \quad \Delta_\rho N_{j0} = 0\,, \tag{4.38}$$
$$\Phi_{j0}'(0) = N_{j0}'(0) = 0\,; \quad \Phi_{j0} \to 0, \quad N_{j0} \to B_{j0} \quad \text{as} \quad \rho \to \infty\,. \tag{4.39}$$

The solution of this system in terms of the linear operator $\mathcal{L}_0$ of Chapter 3, defined by $\mathcal{L}_0\phi = \Delta\phi - \phi + 2\omega\phi$, is simply

$$\mathcal{L}_0\Phi_{j0} = \lambda\Phi_{j0} - \frac{B_{j0}}{f\chi_0^2}\omega^2\,, \qquad N_{j0} = B_{j0}\,, \tag{4.40}$$
$$\Rightarrow \quad \mathcal{L}_0\boldsymbol{\Phi}_0 = \lambda\boldsymbol{\Phi}_0 - \frac{\omega^2}{f\chi_0^2}\boldsymbol{B}_0\,, \qquad \boldsymbol{N}_0 = \boldsymbol{B}_0\,.$$

Moreover, to leading order from the matching condition (4.36), we conclude that

$$(I + \mu\mathcal{E})\boldsymbol{C}_0 = -\boldsymbol{B}_0\,, \qquad \mu \equiv \frac{2\pi D_0 N}{\tau\lambda|\Omega|}\,. \tag{4.41}$$

At the next order, we obtain from (4.25) that the equation for $N_{j1}$ is

$$\Delta_\rho N_{j1} + (1 - 2U_{j0}V_{j0})\Phi_{j0} - U_{j0}^2 N_{j0} = 0\,,$$
$$N_{j1}'(0) = 0\,; \quad N_{j1} \to C_{j0}\ln\rho + B_{j1}\,, \quad \text{as} \quad \rho \to \infty\,.$$

Upon integrating this equation, and using the divergence theorem, we obtain the consistency condition that

$$C_{j0} = \frac{b}{f^2\chi_0^2}B_{j0} - \int_0^\infty \left(1 - 2\frac{\omega}{f}\right)\Phi_{j0}\rho\,d\rho\,, \tag{4.42}$$
$$\Rightarrow \quad \boldsymbol{C}_0 = \frac{b}{f^2\chi_0^2}\boldsymbol{B}_0 - \int_0^\infty \left(1 - 2\frac{\omega}{f}\right)\boldsymbol{\Phi}_0\rho\,d\rho\,.$$

We want to eliminate the $\int_0^\infty \mathbf{\Phi}_0 \rho \, d\rho$ term as before by integrating the equation for $\mathbf{\Phi}_0$ in (4.40). This yields that

$$(\lambda + 1) \int_0^\infty \mathbf{\Phi}_0 \rho d\rho = 2 \int_0^\infty \omega \mathbf{\Phi}_0 \rho \, d\rho + \frac{b}{f\chi_0^2} \boldsymbol{B}_0 \, . \tag{4.43}$$

Then, upon combining (4.41), (4.42) and (4.43), we conclude that

$$[(1+a)I + a\mu\mathcal{E}]\boldsymbol{B}_0 = -\frac{2(\lambda + 1 - f)}{f(\lambda + 1)}(I + \mu\mathcal{E}) \int_0^\infty \omega \mathbf{\Phi}_0 \rho \, d\rho \, , \tag{4.44}$$

where $a \equiv \frac{b(\lambda+1-f)}{f^2\chi_0^2(\lambda+1)}$. Using the fact that $(I + k\mathcal{E})^{-1} = I - \frac{k}{k+1}\mathcal{E}$, we get

$$\boldsymbol{B}_0 = -2m \left(1 + \frac{bm}{f\chi_0^2}\right)^{-1} \left(I + \frac{\mu}{\tau\lambda} \frac{1}{1 + \frac{bm}{f\chi_0^2}(1 + \frac{\mu}{\tau\lambda})} \mathcal{E}\right) \int_0^\infty \omega \mathbf{\Phi}_0 \rho \, d\rho \, , \tag{4.45}$$

where $m$ is defined as $m \equiv \frac{1}{f} - \frac{1}{\lambda+1}$. Upon substituting this expression back into $\mathcal{L}_0 \mathbf{\Phi}_0 = \lambda \mathbf{\Phi}_0 - \frac{\omega^2}{f\chi_0^2} \boldsymbol{B}_0$, we get a vector nonlocal eigenvalue problem (NLEP).

Next, we will decompose $\mathbf{\Phi}_0$ into certain directions, most of which are unaffected by the matrix $\mathcal{E}$. We observe that the geometric meaning of the matrix $\mathcal{E}$ is that of projecting a vector into the direction $\boldsymbol{e} = (1, 1, ..., 1)^T$. This suggests that we decompose $\mathbf{\Phi}_0$ into $k\boldsymbol{e} + \boldsymbol{r}$, where $k$ is some constant and $\boldsymbol{r} \perp \boldsymbol{e}$. Recall from (4.16) that the eigenvectors of the Neumann Green matrix $\mathcal{G}$ are such that $\frac{1}{\sqrt{N}}\boldsymbol{e}$, $\{\boldsymbol{q}_j\}_{j=2}^N$ forms a orthonormal basis of $\mathbf{R}^N$ and $\boldsymbol{q}_j \perp \boldsymbol{e}$ for $j = 2, 3, ..., N$. We decompose $\mathbf{\Phi}_0$ into this basis by writing

$$\mathbf{\Phi}_0(|\boldsymbol{x}|) = k(|\boldsymbol{x}|)\boldsymbol{e} + \sum_{j=2}^{N} u_j(|\boldsymbol{x}|)\boldsymbol{q}_j \, , \tag{4.46}$$

where $k(|\boldsymbol{x}|)$, $u_j(|\boldsymbol{x}|)$ are radially symmetric coefficient functions. Upon substituting this into the equation for $\mathbf{\Phi}_0$, and by using the formula for $\boldsymbol{B}_0$,

we obtain the two distinct NLEP's

$$\mathcal{L}_0 k(|\boldsymbol{x}|) - \frac{2b(\lambda+1-f)(\tau\lambda+\mu)}{(\lambda+1)f^2\chi_0^2\tau\lambda + b(1-f+\lambda)(\tau\lambda+\mu)} \frac{\int_0^\infty k\omega\rho\, d\rho}{\int_0^\infty \omega^2\rho\, d\rho}\omega^2 = \lambda k(|\boldsymbol{x}|)\,,$$
$$\mathcal{L}_0 u_j - \frac{2b(\lambda+1-f)}{(\lambda+1)f^2\chi_0^2 + b(1-f+\lambda)} \frac{\int_0^\infty u_j\omega\rho\, d\rho}{\int_0^\infty \omega^2\rho\, d\rho}\omega^2 = \lambda u_j\,. \tag{4.47}$$

These two distinct NLEP's are similar to those considered previously. As such we conclude that the component $k(|\boldsymbol{x}|)$ is linearly stable, but that there is a stability threshold for $u_j(|\boldsymbol{x}|)$ when

$$\beta(\lambda)|_{\lambda=0} = \frac{2b(\lambda+1-f)}{(\lambda+1)f^2\chi_0^2 + b(1-f+\lambda)}|_{\lambda=0} = 1\,,$$

which yields that

$$\chi_0^2 = \frac{(1-f)b}{f^2}\,, \qquad S_{c0} = \frac{\sqrt{b(1-f)}}{f}\,. \tag{4.48}$$

We remark here that at the stability threshold we have $\lambda = 0$, which seems to contradict our starting assumption $\lambda \neq 0$. However, the previous theorem of [16], states that when $\beta(0) < 1$ the NLEP has a positive real eigenvalue. Another difficulty is that near the stability threshold the eigenvalue can be very small. In particular, if $\lambda = \mathcal{O}(\nu)$, then the $\frac{2\pi\nu DN}{\tau\lambda|\Omega|}\mathcal{E}$ term in the matching condition (4.36) becomes the dominate term and the asymptotic expansions need a little modification. We will handle these two situations in Section 4.2.2 and Section 4.2.3, respectively.

### 4.2.2 $\lambda \sim \mathcal{O}(\nu)$ and $\lambda \neq 0$

Next we treat the case where $\lambda \sim \mathcal{O}(\nu)$ and $\lambda \neq 0$, and we expand $\lambda$ as $\lambda = \nu\lambda_1 + \nu^2\lambda_2 + ....$ For this case the results (4.27), (4.28), and (4.31) still hold. However, the only difference is that the $\frac{D}{\tau\lambda|\Omega|}$ term is no longer $\mathcal{O}(\nu^{-1})$, but instead is $\mathcal{O}(\nu^{-2})$. This implies that the matching condition is modified as

$$\left(\frac{2\pi D_0 N}{\tau\lambda_1|\Omega|}\mathcal{E} + \nu I + 2\pi\nu^2\mathcal{G}\right)\boldsymbol{C} = -\nu^2\boldsymbol{B}\,. \tag{4.49}$$

Since the system is linear, then without loss of generality we may assume that $\boldsymbol{B} \sim \mathcal{O}(\nu)$ and from (4.49) it seems that $\boldsymbol{C} \sim \mathcal{O}(\nu^2)$. However, this scaling assumption would be inconsistent with the logarithmic growth condition in the equation for $N_{j1}$. In fact, the leading-order solution to (4.49 is that $\mathcal{E}\boldsymbol{C} = \boldsymbol{0}$, which is equivalent to $\boldsymbol{C} \perp \boldsymbol{e}$. We then expand the solutions as in (4.37) and obtain that the matching condition becomes

$$(I + 2\pi\nu\mathcal{G})\boldsymbol{C} = -\nu\boldsymbol{B}\,. \tag{4.50}$$

Due to the properties of $\mathcal{G}$ in (4.16), it follows that $\boldsymbol{B} \perp \boldsymbol{e}$. Therefore, at leading order, we have

$$\boldsymbol{B}_0 = -\boldsymbol{C}_0 \perp \boldsymbol{e}, \quad \mathcal{L}_0\boldsymbol{\Phi}_0 = -\frac{\omega^2}{f\chi_0^2}\boldsymbol{B}_0, \quad \boldsymbol{N}_0 = \boldsymbol{B}_0, \quad \Rightarrow \quad \boldsymbol{\Phi}_0 = -\frac{\omega}{f\chi_0^2}\boldsymbol{B}_0\,. \tag{4.51}$$

We may assume that $\boldsymbol{C}_0 = \sum_{j=2}^{N} d_j \boldsymbol{q}_j = -\boldsymbol{B}_0$, where $\boldsymbol{q}_j$ are other eigenvectors of $\mathcal{G}$ that are orthogonal to $\boldsymbol{e}$ and $d_j$ are some constant coefficients. At next order, the equation for $\boldsymbol{N}_1$ is:

$$\begin{aligned} &\Delta\boldsymbol{N}_1 = \frac{\omega}{f\chi_0^2}\boldsymbol{B}_0 - \frac{\omega^2}{f^2\chi_0^2}\boldsymbol{B}_0\,, \\ &\boldsymbol{N}_1'(0) = 0\,, \quad \boldsymbol{N}_1 \to \boldsymbol{C}_0 \ln|\boldsymbol{y}| + \boldsymbol{B}_1\,, \quad \text{as} \quad |\boldsymbol{y}| \to \infty\,. \end{aligned} \tag{4.52}$$

The solvability condition for this equation gives:

$$\boldsymbol{C}_0 = \frac{b}{f\chi_0^2}(1 - \frac{1}{f})\boldsymbol{B}_0 = -\boldsymbol{B}_0, \quad \Rightarrow \quad \chi_0 = \sqrt{\frac{b(1-f)}{f^2}}\,, \quad S_0 = \frac{\sqrt{b(1-f)}}{f}\,, \tag{4.53}$$

which is precisely the same threshold we obtained from (4.47). The solution to (4.52) can then be written as

$$\boldsymbol{N}_1 = \boldsymbol{B}_1 - \frac{V_{1P}}{b(1-f)}\boldsymbol{B}_0 = \boldsymbol{B}_1 + \frac{V_{1P}}{b(1-f)}\sum_{j=2}^{N} d_j\boldsymbol{q}_j\,. \tag{4.54}$$

Upon substituting this expression into the equation for $\boldsymbol{N}_2$ we get

$$\begin{aligned}
&\Delta \boldsymbol{N}_2 + (1 - \frac{2\omega}{f})\boldsymbol{\Phi}_1 - 2\left(\frac{\omega}{f\chi_0}(\chi_1 + \frac{V_{1P}}{f^2\chi_0}) + \chi_0(-\frac{\chi_1}{f\chi_0^2}\omega - \frac{U_{1P}}{f^3\chi_0^3})\right)\boldsymbol{\Phi}_0 \\
&\quad - \frac{\omega^2}{f^2\chi_0^2}\boldsymbol{N}_1 - 2\frac{\omega}{f\chi_0^2}(-\frac{\chi_1}{f\chi_0^2}\omega - \frac{U_{1P}}{f^3\chi_0^3})\boldsymbol{N}_0 = 0\,, \\
&\boldsymbol{N}_2'(0) = \boldsymbol{0}\,, \quad \boldsymbol{N}_2 \to \boldsymbol{C}_1 \ln|\boldsymbol{y}| + \boldsymbol{B}_2\,, \quad \text{as} \quad |\boldsymbol{y}| \to \infty\,.
\end{aligned}$$

Upon using the divergence theorem on this equation for $N_2$, and by using (4.51) and (4.54), we obtain that the following consistency condition must hold:

$$\begin{aligned}
&\boldsymbol{C}_1 + \int_0^\infty \boldsymbol{\Phi_1}\rho d\rho - \frac{2\omega}{f}\int_0^\infty \boldsymbol{\Phi_1}\rho\, d\rho - \frac{1}{1-f}\boldsymbol{B}_1 - \frac{3}{b^2(1-f)^2}\int_0^\infty \omega^2 V_{1P}\rho\, d\rho \\
&\sum_{j=2}^N d_j\boldsymbol{q}_j - 2\frac{f\chi_1}{b^{\frac{1}{2}}(1-f)^{\frac{3}{2}}}\sum_{j=2}^N d_j\boldsymbol{q}_j = \boldsymbol{0}\,. \qquad (4.55)
\end{aligned}$$

Similarly, the matching condition (4.50) gives

$$\boldsymbol{C}_1 + 2\pi\mathcal{G}\boldsymbol{C}_0 = -\boldsymbol{B}_1, \quad \Rightarrow \quad \boldsymbol{C}_1 + 2\pi\sum_{j=2}^N k_j d_j \boldsymbol{q}_j = -\boldsymbol{B}_1. \qquad (4.56)$$

The equation for $\boldsymbol{\Phi}_1$ then becomes

$$\begin{aligned}
&\mathcal{L}_0\boldsymbol{\Phi}_1 + \frac{3f\omega^2 V_{1p}}{b^2(1-f)^2}\sum_{j=2}^N d_j\boldsymbol{q}_j + \frac{2f^2\chi_1\omega^2}{(b(1-f))^{\frac{3}{2}}}\sum_{j=2}^N d_j\boldsymbol{q}_j \qquad (4.57)\\
&\qquad + \frac{f\omega^2}{b(1-f)}\boldsymbol{B}_1 = \lambda_1\frac{f}{b(1-f)}\omega\sum_{j=2}^N d_j\boldsymbol{q}_j\,.
\end{aligned}$$

Upon integrating this equation and then substituting into (4.55) and (4.56), we get that

$$\boldsymbol{B}_1 = \pi\sum_{j=2}^N d_j k_j \boldsymbol{q}_j - \frac{1-f}{f}\int_0^\infty \omega\boldsymbol{\Phi}_1\rho\, d\rho$$

$$-\frac{f}{b(1-f)}\sum_{j=2}^{N} d_j \boldsymbol{q}_j \left(\frac{b\chi_1(1-f)}{f\chi_0}+\frac{3}{2bf}\int_0^\infty \omega^2 V_{1P}\rho\, d\rho+\frac{b}{2}\lambda_1\right).$$

Finally, we substitute this expression back into (4.57) to obtain the vector NLEP

$$\mathcal{L}\boldsymbol{\Phi}_1 \equiv \mathcal{L}_0\boldsymbol{\Phi}_1-\frac{\int_0^\infty \boldsymbol{\Phi}_1\omega\rho\, d\rho}{\int_0^\infty \omega^2\rho\, d\rho}\omega^2=\lambda_1(\omega+\frac{f}{2-2f}\omega^2)\frac{f}{b(1-f)}\sum_{j=2}^{N} d_j\boldsymbol{q}_j$$
$$-\frac{3f\omega^2 V_{1P}}{b^2(1-f)^2}\sum_{j=2}^{N} d_j\boldsymbol{q}_j-\frac{f}{b(1-f)}\sum_{j=2}^{N} d_j\boldsymbol{q}_j\left(-\pi k_j+\frac{\chi_1}{\chi_0}-\frac{3\int_0^\infty \omega^2 V_{1P}\rho\, d\rho}{2b^2(1-f)}\right)\omega^2.$$

Upon decomposing $\boldsymbol{\Phi}_1(\boldsymbol{x})=r(\boldsymbol{x})\boldsymbol{e}+\sum_{j=2}^{N} t_j(\boldsymbol{x})\boldsymbol{q}_j$ as before, we obtain that the coefficient functions $t_j(\boldsymbol{x})$ satisfy

$$\mathcal{L}t_j(\boldsymbol{x})=\frac{fd_j}{b(1-f)}\{\lambda_1(\omega+\frac{f}{2-2f}\omega^2)-\frac{3}{b(1-f)}\omega^2 V_{1P}$$
$$-\omega^2\left(-\pi k_j+\frac{\chi_1}{\chi_0}-\frac{3}{2b^2(1-f)}\int_0^\infty \omega^2 V_{1P}\rho\, d\rho\right)\}.$$

Finally, we use a solvability condition on this problem to calculate $\lambda_1$. From Section 3.2 the adjoint operator $\mathcal{L}^*$ has a one-dimensional nullspace $\Psi^*(\boldsymbol{x})$ in the class of radially symmetric functions, where $\Psi^\star = w+\rho w'/2$ was given in Section 3.2. We then impose the solvability condition as similar to that done in Section 3.2 to conclude that

$$\int_0^\infty RHS\cdot\Psi^*\rho\, d\rho=0 \;\Rightarrow\; \lambda_1=2(1-f)\left(-\pi k_j+\frac{\chi_1}{\chi_0}+\frac{3\int_0^\infty U_{1P}\rho\, d\rho}{2(1-f)b^2}\right)$$
$$=2(1-f)\left(-\pi k_j-\frac{S_1}{S_0}+\frac{\int_0^\infty U_{1P}\rho\, d\rho}{2(1-f)b^2}\right).$$

With this expression we can calculate the next order term in the stability threshold that makes $\lambda_1=0$ as

$$S_{c1}=\max_{2\le j\le N}\{\frac{S_0}{2}(-2\pi k_j+\frac{1}{(1-f)b^2}\int_0^\infty U_{1P}\rho\, d\rho)\}=\max_{2\le j\le N}\{\frac{\sqrt{b(1-f)}}{2f}$$

$$(-2\pi k_j + \frac{1}{(1-f)b^2}((1-f)\int_0^\infty U_{1QII}\rho\, d\rho - \int_0^\infty U_{1QI}\rho\, d\rho))\}\,. \tag{4.58}$$

We remark here that since $\mathcal{G}$ is real symmetric, all of its eigenvalues $k_j$ are real. Therefore, as expected, the stability threshold is real-valued.

### 4.2.3 $\lambda$=0

Finally we consider the case where $\lambda = 0$, which corresponding to the stability threshold. The equation for $\eta$ now becomes

$$\Delta\eta = 2\pi \sum_{j=1}^{N} C_j \delta(\boldsymbol{x} - \boldsymbol{x}_j)\,. \tag{4.59}$$

As we mentioned before, if we integrate this PDE with the no-flux boundary conditions on $\partial\Omega$, we obtain that

$$\sum_{j=1}^{N} C_j = 0\,, \qquad \eta(\boldsymbol{x}) = -2\pi \sum_{j=1}^{N} C_j G_0(\boldsymbol{x}, \boldsymbol{x}_j)\,, \tag{4.60}$$

where $G_0(\boldsymbol{x}, \boldsymbol{x}_j)$ is the Neumann Green function defined as before. Using the same method in Section 3.3, we derive that $\frac{\partial}{\partial S}U_j(\boldsymbol{y}, S_j)$, $\frac{\partial}{\partial S}V_j(\boldsymbol{y}, S_j)$ are solutions to (4.25) when $\lambda = 0$. This leads to the relation

$$\frac{B_j}{C_j} = \frac{\partial}{\partial S}\chi(S_j, f)\,. \tag{4.61}$$

Since we are assuming a common source strength $S_j = S = S_c$, (4.61) gives $\boldsymbol{B} = \frac{\partial}{\partial S}\chi(S_c, f)\boldsymbol{C}$. We substitute this expression back into the matching condition (4.36) and, upon noticing that $\mathcal{E}\boldsymbol{C} = \boldsymbol{0}$, we have

$$(I + \nu\frac{\partial\chi}{\partial S}(S_c, f))\boldsymbol{C} = -2\pi\nu\mathcal{G}\boldsymbol{C}\,. \tag{4.62}$$

This implies that $\boldsymbol{C}$ is an eigenvector of $\mathcal{G}$, and we obtain the relation

$$1 + \nu\frac{\partial\chi}{\partial S}(S_c, f) = -2\pi\nu k_j\,. \tag{4.63}$$

As we derived in (3.64) and (3.65), we calculate

$$\frac{\partial}{\partial S}\chi(S_c, f) = -\frac{1}{\nu}\frac{b(1-f)}{f^2}\frac{1}{S_{c0}^2} + (2\frac{b(1-f)}{f^2}\frac{S_{c1}}{S_{c0}^3} - \frac{\int_0^\infty U_{1P}\rho\, d\rho}{(1-f)b^2}) + \mathcal{O}(\nu)\,. \tag{4.64}$$

We substitute this expression back into (3.63) and equate terms of a common order in $\nu$. In this way, we derive the stability threshold results

$$S_{c0} = \frac{\sqrt{b(1-f)}}{f}\,, \tag{4.65}$$

$$\begin{aligned} S_{c1} = \max_{2\le j\le N}\{&\frac{\sqrt{b(1-f)}}{2f}(-2\pi k_j + \frac{1}{(1-f)b^2} \\ &((1-f)\int_0^\infty U_{1QII}\rho\, d\rho - \int_0^\infty U_{1QI}\rho\, d\rho))\}\,. \end{aligned}$$

Finally, by using (4.15) which relates $S$ to $D$, we calculate the stability threshold in terms of $D$. The results are summarized as follows:

**Principal Result 5.** *In the limit $\epsilon \to 0$, and on the range $D \sim \mathcal{O}(\frac{1}{\nu})$, the multi-spot patterns constructed in Principal Result 4 are linearly stable if*

$$D < D_c = \frac{D_{c0}}{\nu} + D_{c1} + \dots\,, \tag{4.66}$$

*where $D_{c0}$ and $D_{c1}$ are defined by*

$$D_{c0} = \frac{f^2E^2|\Omega|^2}{4\pi^2N^2(1-f)b}\,, \tag{4.67}$$

$$D_{c1} = \min_{2\le j\le N}\{D_{c0}(2\pi k_j - \frac{1}{(1-f)b^2}\int_0^\infty U_{1P}\rho\, d\rho)\} \tag{4.68}$$

$$= \min_{2\le j\le N}\{D_{c0}(2\pi k_j + \frac{1}{(1-f)b^2}\int_0^\infty U_{1QI}\rho\, d\rho - \frac{1}{b^2}\int_0^\infty U_{1QII}\rho\, d\rho)\}\,. \tag{4.69}$$

We remark here that since we are solving for eigenvalues of a self-adjoint operator, all the eigenvalues are real-valued, and so the stability threshold is real. Although we have discussed the three cases of $\lambda$ separately, the analysis indeed provides a uniform transition between the ranges of $\lambda$. More specif-

ically, we obtain the same leading order results for the stability threshold from (4.48), (4.53) and (4.65). Moreover, (4.58) also agrees with (4.65) at second order. Finally, in Section 4.2.2, we must have $\sum_{j=1}^{N} C_j = 0$ to have a solution, which also agrees with the solvability condition in Section 4.2.3.

# Chapter 5

# Numerical Results

In this chapter, we perform some numerical experiments and compare the results with the two term asymptotic approximations for the stability threshold derived in the previous chapter. For the periodic case, we will identify the optimal lattice arrangement of spots. For the finite domain problem we illustrate our theory for the case of equally-spaced spots on a ring that is concentric with the unit disk. For this finite domain problem, there is an explicit formula for the Neumann Green function that will be used.

## 5.1 Small $S$ Asymptotics of $\chi(S, f)$

For both the periodic and the finite domain problems, the same core problems (3.3) and (4.4) arise in the asymptotic construction of the spot pattern. In these common inner problems, a key quantity is $\chi(S, f)$, which appears in the asymptotic boundary condition. Two-term asymptotic expansions for $\chi(S, f)$ have been derived previously in Principal Result 1 and Principal Result 4. We now solve the core problem numerically to compute the $\chi(S, f)$, and we compare the numerical results for $\chi(S, f)$ with the corresponding two-term asymptotic results derived in the small $S$ limit.

Since we are seeking radially symmetric solutions, solving the core problem is actually solving an ODE system. We use the ODE boundary value problem solver BVP4C in Matlab. We now remark on a few details of the numerical implementation.

- The Laplace operator in $\mathbf{R}^2$ polar coordinates is expressed as:

$$\Delta_\rho = \frac{d^2}{d\rho^2} + \frac{1}{\rho}\frac{d}{d\rho}\,.$$

- Instead of solving the ODE systems on the whole interval $[0, \infty)$, we use the interval $[\mu, R]$, where $R$ is a sufficiently large number so as to approximate the infinite domain, while $\mu$ is a sufficiently small number to avoid the singularity at $r = 0$. We chose $R = 15$ and $\mu = 0.005$ in our computations.

- Instead of using the boundary conditions for $U(\rho)$ and $V(\rho)$ as $\rho \to \infty$ in (3.4) directly, we set $U(R) = 0$ and $V^{'}(R) \sim \frac{S}{R}$. Then, after solving the core problem numerically, we define $\chi(S, f)$ by $\chi(S, f) = V(R) - S \ln R$.

- The boundary value solver requires a good initial guess consistent with the boundary conditions. First we may want to use our small $S$ asymptotic approximation in Principal Result 1 as an initial guess. To do this, we in principle need to know the radially symmetric solution of $\Delta\omega - \omega + \omega^2 = 0$ in $\mathbf{R}^2$. However, this explicit solution is not available in $\mathbf{R}^2$, and is only available in $\mathbf{R}^1$. As such, we adapt a homotopy algorithm to find the initial guess. For a fixed $f$, we first start with a small $S_0$, and use the asymptotic approximation for the core problem in $\mathbf{R}$. We then slowly increase the dimension from 1 to 2 and solve the core problem using the previous step as an initial guess. After having obtained the core solution for $S = S_0$ in $\mathbf{R^2}$ using this homotopy strategy, we then increase $S$ and solve the core problem based on the previously computed solution.

After computing the $\chi(S, f)$ in this way, we compare the results with the two term asymptotic expansions in (3.64). In the asymptotic approximation, we require numerical values for a few integrals. We obtain that $b \approx \int_0^\infty \omega\rho d\rho = 4.9343$, $\int_0^\infty U_{1QI}\rho d\rho \approx 11.9131$ and $\int_0^\infty U_{1QI}\rho\, d\rho \approx 11.4384$. Figure 5.1 shows results for $f = 0.4$ and $f = 0.5$, where the green (top) curves are the asymptotic approximations and the blue (bottom) curves are the full numerical results. We observe that the two curves are rather close for small $S$, which is what we should expect.

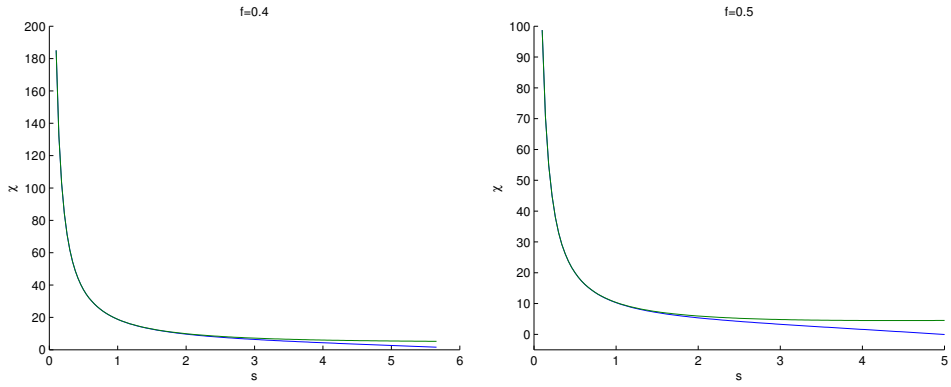


Figure 5.1: Numerical solution (bottom curves) and asymptotic results (top curves) for $\chi(S, f)$. In the left panel we fix $f = 0.4$, while $f = 0.5$ for the right panel. In both pictures, the blue (bottom) curve is the numerical solution while the green (top) one is the two term asymptotic expansion.

## 5.2 Stability Threshold and the Optimal Lattice Arrangement

In this section, we compute the stability threshold numerically and compare the results with the two term asymptotic approximation.

As derived in (3.63) and (3.65), the stability threshold for $S$, labeled by $S_c$, for the periodic spot problem is the largest $S$, corresponding to the smallest $D$, that solves the transcendental equation

$$\frac{\partial}{\partial S}\chi(S_c, f) = -\frac{1}{\nu} - 2\pi R_{0,\boldsymbol{k}} + \mathcal{O}(\nu)\,, \tag{5.1}$$

for some Bloch vector $\boldsymbol{k}$ in the first Brillouin zone. For the corresponding finite domain problem, the stability threshold is the largest $S$ that solves

$$\frac{\partial}{\partial S}\chi(S_c, f) = -\frac{1}{\nu} - 2\pi k_i\,, \tag{5.2}$$

for certain eigenvalues $k_i$ of the Neumann Green matrix.

Since we have already computed $\chi(S, f)$ above, we can use a cubic spline

and a numerical derivative to get $\frac{\partial}{\partial S}\chi(S,f)$. Then we use a nonlinear equation solver to compute the threshold directly.

On the other hand, we have derived the two term asymptotic approximation for the stability threshold in both cases. For the periodic case, we derived previously that

$$S_c = \nu^{\frac{1}{2}}\frac{\sqrt{b(1-f)}}{f}(1+\nu(\frac{1}{2b^2}\int_0^\infty U_{1QII}\rho\,d\rho - \frac{1}{2b^2(1-f)}\int_0^\infty U_{1QI}\rho\,d\rho - \pi \min_{\boldsymbol{k}\in\Omega^*\setminus\mathbf{0}} R_{0,\boldsymbol{k}}))\,, \tag{5.3}$$

while for the finite domain problem we derived that

$$S_c = \nu^{\frac{1}{2}}\frac{\sqrt{b(1-f)}}{f}(1+\nu(\frac{1}{2b^2}\int_0^\infty U_{1QII}\rho\,d\rho - \frac{1}{2b^2(1-f)}\int_0^\infty U_{1QI}\rho\,d\rho - \pi \min_{2\le i\le N} k_i))\,. \tag{5.4}$$

Notice that the only key difference between these two expressions is that $\min_{\boldsymbol{k}\in\Omega^*\setminus\mathbf{0}} R_{0,\boldsymbol{k}}$ is replaced by $\min_{2\le i\le N} k_i$. Therefore, we introduce a parameter $c$ and our goal is to compare the solution to

$$\frac{\partial}{\partial S}\chi(S_c,f) = -\frac{1}{\nu} - c\,, \tag{5.5}$$

with the expression

$$S_c = \nu^{\frac{1}{2}}\frac{\sqrt{b(1-f)}}{f}\left(1+\nu(\frac{1}{2b^2}\int_0^\infty U_{1QII}\rho\,d\rho - \frac{1}{2b^2(1-f)}\int_0^\infty U_{1QI}\rho\,d\rho - \frac{c}{2})\right),$$

for some small $\epsilon$. In Figure 5.2 we show numerical results that confirm that the full numerical results and asymptotic results agree rather well.

Next, we identify the optimal lattice arrangement for the periodic case. As stated in Principal Result 3, the optimal lattice arrangement $\Lambda_{op}$ with fixed primitive cell of area unity is the one which solve the following max-min problem:

$$\arg\max_{\Lambda,\ |\Omega|=1}\{\min_{\boldsymbol{k}\in\Omega^*\setminus\mathbf{0}}\{R_{0,\boldsymbol{k}}\}\} \tag{5.6}$$

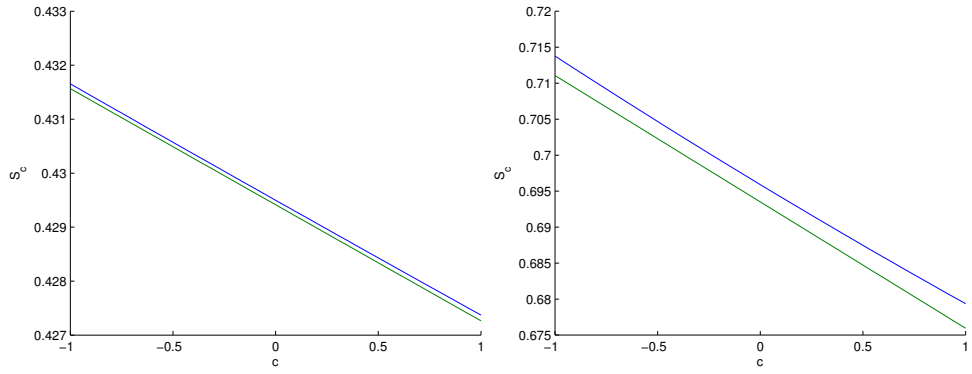


Figure 5.2: Numerical solution to (5.5) and the two-term asymptotic approximations for $S_c$ with different $c$. Left panel: $f = 0.4$ and $\epsilon = 0.01$. Right panel: $f = 0.5$ and $\epsilon = 0.05$. The blue (top) curve is the numerical solution while the green (bottom) one is the asymptotic approximations in both cases.

Therefore, if we want to find the optimal lattice numerically, we need to know how to calculate $R_{0,\boldsymbol{k}}$. First we follow the process in [2] and [8], to derive an explicit expression for the Bloch Green function and its regular part $R_{0,\boldsymbol{k}}$. Recall that the Bloch Green function satisfies:

$$\begin{aligned}
&\Delta G_{0,\boldsymbol{k}}(\boldsymbol{x}) = -\delta(\boldsymbol{x}), \quad \forall \boldsymbol{x} \in \Omega\,,\\
&G_{0,\boldsymbol{k}}(\boldsymbol{x}+\boldsymbol{L}_i) = e^{-\mathrm{i}\boldsymbol{k}\cdot\boldsymbol{L}_i} G_{0,\boldsymbol{k}}(\boldsymbol{x})\,, \quad \forall \boldsymbol{x} \in \boldsymbol{d}_{-i}\,,\\
&\partial_{\boldsymbol{n}-} G_{0,\boldsymbol{k}}(\boldsymbol{x}+\boldsymbol{L}_i) = e^{-\mathrm{i}\boldsymbol{k}\cdot\boldsymbol{L}_i} \partial_{\boldsymbol{n}+} G_{0,\boldsymbol{k}}(\boldsymbol{x})\,, \quad \forall \boldsymbol{x} \in \boldsymbol{d}_{-i}\,.
\end{aligned}$$

The free space Green's function in the absence of any boundary conditions is $G_{free}(\boldsymbol{x}) = -\frac{1}{2\pi}\ln|\boldsymbol{x}|$. We then observe that the infinite sum

$$G(\boldsymbol{x}) = \sum_{\boldsymbol{l}\in\Lambda} G_{free}(\boldsymbol{x}+\boldsymbol{l}) e^{i\boldsymbol{k}\cdot\boldsymbol{l}}\,,$$

satisfies the PDE together with the quasi-periodic boundary conditions. To

verify that it satisfies these boundary conditions we calculate

$$\begin{aligned} G(\boldsymbol{x}+\boldsymbol{L}_i) &= \sum_{\boldsymbol{l}\in\Lambda} G_{free}(\boldsymbol{x}+\boldsymbol{L}_i+\boldsymbol{l})e^{i\boldsymbol{k}\cdot\boldsymbol{l}}\,, \\ &= \sum_{\boldsymbol{L}_i+\boldsymbol{l}\in\Lambda} G_{free}(\boldsymbol{x}+(\boldsymbol{L}_i+\boldsymbol{l}))e^{i\boldsymbol{k}\cdot(\boldsymbol{L}_i+\boldsymbol{l})}e^{i\boldsymbol{k}\cdot(-\boldsymbol{L}_i)}\,, \\ &= e^{-i\boldsymbol{k}\cdot\boldsymbol{L}_i}\sum_{\boldsymbol{l}'\in\Lambda} G_{free}(\boldsymbol{x}+\boldsymbol{l}')e^{i\boldsymbol{k}\cdot\boldsymbol{l}'} = e^{-i\boldsymbol{k}\cdot\boldsymbol{L}_i}G(\boldsymbol{x})\,. \end{aligned}$$

The second line above follows since $\boldsymbol{L}_i \in \Lambda$ and $\boldsymbol{l}' = \boldsymbol{L}_i + \boldsymbol{l}$.

By the Poisson summation formula proved in (2.4) in Chapter 2, and the fact that $\widehat{G_{free}}(\boldsymbol{\xi}) = \frac{1}{|\boldsymbol{\xi}|^2}$ and $|\Omega| = 1$, we have

$$G(\boldsymbol{x}) = \sum_{\boldsymbol{l}\in\Lambda} G_{free}(\boldsymbol{x}+\boldsymbol{l})e^{i\boldsymbol{k}\cdot\boldsymbol{l}} = \sum_{\boldsymbol{d}\in\Lambda^*} \widehat{G_{free}}(\boldsymbol{d}-\boldsymbol{k})e^{i\boldsymbol{x}\cdot(\boldsymbol{d}-\boldsymbol{k})} = \sum_{\boldsymbol{d}\in\Lambda^*} \frac{e^{i\boldsymbol{x}\cdot(\boldsymbol{d}-\boldsymbol{k})}}{|\boldsymbol{d}-\boldsymbol{k}|^2}\,.$$

It is easy to prove from an integral test that the last series is not absolutely convergent. However, we can show it is actually conditionally convergent for $\boldsymbol{x} \neq \boldsymbol{0}$ by decomposing it into two parts as was done in [2]. We pick some $\eta$ in $\eta \in (0,1)$, and rewrite the infinite series as

$$\begin{aligned} \sum_{\boldsymbol{d}\in\Lambda^*} \frac{e^{i\boldsymbol{x}\cdot(\boldsymbol{d}-\boldsymbol{k})}}{|\boldsymbol{d}-\boldsymbol{k}|^2} &= \sum_{\boldsymbol{d}\in\Lambda^*} \frac{e^{i\boldsymbol{x}\cdot(\boldsymbol{d}-\boldsymbol{k})}}{|\boldsymbol{d}-\boldsymbol{k}|^2}(1-e^{-\frac{|\boldsymbol{d}-\boldsymbol{k}|^2}{4\eta^2}}+e^{-\frac{|\boldsymbol{d}-\boldsymbol{k}|^2}{4\eta^2}})\,, \\ &= \sum_{\boldsymbol{d}\in\Lambda^*} \frac{e^{i\boldsymbol{x}\cdot(\boldsymbol{d}-\boldsymbol{k})}}{|\boldsymbol{d}-\boldsymbol{k}|^2}e^{-\frac{|\boldsymbol{d}-\boldsymbol{k}|^2}{4\eta^2}} + \sum_{\boldsymbol{d}\in\Lambda^*} \frac{e^{i\boldsymbol{x}\cdot(\boldsymbol{d}-\boldsymbol{k})}}{|\boldsymbol{d}-\boldsymbol{k}|^2}(1-e^{-\frac{|\boldsymbol{d}-\boldsymbol{k}|^2}{4\eta^2}})\,. \end{aligned}$$

The first term is an absolutely convergent series, which we denote as

$$G_{Fourier}(\boldsymbol{x}) = \sum_{\boldsymbol{d}\in\Lambda^*} \frac{e^{i\boldsymbol{x}\cdot(\boldsymbol{d}-\boldsymbol{k})}}{|\boldsymbol{d}-\boldsymbol{k}|^2}e^{-\frac{|\boldsymbol{d}-\boldsymbol{k}|^2}{4\eta^2}}\,. \tag{5.7}$$

We claim that the second term equals another absolutely convergent series over the original lattice $\Lambda$. We can write this series in a convenient form using the following lemma:

**Lemma 5.**

$$\sum_{\boldsymbol{d}\in\Lambda^*}\frac{e^{i\boldsymbol{x}\cdot(\boldsymbol{d}-\boldsymbol{k})}}{|\boldsymbol{d}-\boldsymbol{k}|^2}(1-e^{-\frac{|\boldsymbol{d}-\boldsymbol{k}|^2}{4\eta^2}})=\sum_{\boldsymbol{l}\in\Lambda}F_{sing}(\boldsymbol{x}+\boldsymbol{l})e^{i\boldsymbol{k}\cdot\boldsymbol{l}}\,,\quad\forall\boldsymbol{x}\in\Omega\backslash\boldsymbol{0}\,,\qquad(5.8)$$

*where* $F_{sing}(\boldsymbol{x})\equiv\frac{1}{2\pi}\int_{\ln(2\eta)}^{\infty}e^{-\frac{|\boldsymbol{x}|^2}{4}e^{2s}}\,ds=\frac{1}{4\pi}E_1(\eta^2|\boldsymbol{x}|^2)$*, and* $E_1(z)$ *is the exponential integral defined by* $E_1(z)=\int_z^\infty t^{-1}e^{-t}\,dt$*.*

*Proof.* Firstly, we observe that $\frac{1}{2\pi}\int_{\ln(2\eta)}^{\infty}e^{-\frac{|\boldsymbol{x}|^2}{4}e^{2s}}\,ds=\frac{1}{4\pi}E_1(\eta^2|\boldsymbol{x}|^2)$ by using a simple change of variables. Then, according to [1], the exponential integral $E_1(z)$ has the decay property, $E_1(z)<e^{-z}\ln(1+\frac{1}{z})$, so that the series over $\Lambda$ given by the right hand-side of (5.8) converges absolutely. Then, by using the Poisson summation formula as proved in (2.4), we get

$$\sum_{\boldsymbol{l}\in\Lambda}F_{sing}(\boldsymbol{x}+\boldsymbol{l})e^{i\boldsymbol{k}\cdot\boldsymbol{l}}=\sum_{\boldsymbol{d}\in\Lambda^*}\widehat{F_{sing}}(\boldsymbol{d}-\boldsymbol{k})e^{i\boldsymbol{x}\cdot(\boldsymbol{d}-\boldsymbol{k})}\,.\qquad(5.9)$$

Upon comparing this result with the statement that we want to prove, we need only show that $\widehat{F_{sing}}(\boldsymbol{\xi})=\frac{1}{|\boldsymbol{\xi}|^2}(1-e^{-\frac{|\boldsymbol{\xi}|^2}{4\eta^2}})$. To prove this we show that the inverse Fourier transform of the right hand-side is $F_{sing}(\boldsymbol{x})$. Notice that both $F_{sing}(\boldsymbol{x})$ and the right hand-side are radially symmetric, and that the inverse Fourier transform of a radially symmetric function is the inverse Hankel transform of order zero (cf. [11]), so that $f(r)=(2\pi)^{-1}\int_0^\infty\hat{f}(\rho)J_0(\rho r)\rho\,d\rho$. Upon using the well-known inverse Hankel transform (cf. [11])

$$\int_0^\infty e^{-\rho^2e^{-2s}}\rho J_0(\rho r)\,d\rho=\frac{1}{2}e^{2s-\frac{r^2e^{2s}}{4}}\,,$$

and the fact that

$$\frac{1}{\rho^2}(1-e^{-\frac{\rho^2}{4\eta^2}})=2\int_{\ln(2\eta)}^\infty e^{-\rho^2e^{-2s}-2s}ds\,,$$

we calculate the inverse Fourier transform of $\frac{1}{\rho^2}(1-e^{-\frac{\rho^2}{4\eta^2}})$ as

$$\frac{1}{2\pi}\int_0^\infty(\frac{1}{\rho^2}(1-e^{-\frac{\rho^2}{4\eta^2}}))J_0(\rho r)\rho\,d\rho=\frac{1}{2\pi}\int_0^\infty(\int_{\ln(2\eta)}^\infty 2e^{-\rho^2e^{-2s}-2s}\,ds)J_0(\rho r)\rho\,d\rho$$

$$= \frac{1}{\pi}\int_{\ln(2\eta)}^{\infty} e^{-2s}\left(\int_0^{\infty} e^{-\rho^2 e^{-2s}}\rho J_0(\rho r)\,d\rho\right) ds = \frac{1}{2\pi}\int_{\ln(2\eta)}^{\infty} e^{-2s}e^{2s-\frac{r^2}{4}e^{2s}}\,ds$$
$$= \frac{1}{2\pi}\int_{\ln(2\eta))}^{\infty} e^{-\frac{r^2}{4}e^{2s}}\,ds\,.$$

Thus, we conclude that $\mathcal{F}^{-1}(\frac{1}{|\boldsymbol{\xi}|^2}(1-e^{-\frac{|\boldsymbol{\xi}|^2}{4\eta^2}})) = F_{sing}(\boldsymbol{x})$, which completes the proof of the lemma. □

We remark here that the series over the reciprocal lattice $\Lambda^*$, given by the left hand-side of (5.8), is only conditionally convergent, while the series over the original lattice $\Lambda$, given by the right hand-side of (5.8), converges absolutely and we denote it by

$$G_{spatial}(\boldsymbol{x}) = \sum_{\boldsymbol{l}\in\Lambda} F_{sing}(\boldsymbol{x}+\boldsymbol{l})e^{i\boldsymbol{k}\cdot\boldsymbol{l}}\,. \tag{5.10}$$

In this way, we have an explicit expression for the Bloch Green function $G_{0,\boldsymbol{k}} = G(\boldsymbol{x})$, and have separated it into the sum of two absolutely convergent series as

$$G(\boldsymbol{x}) = G_{Fourier}(\boldsymbol{x}) + G_{spatial}(\boldsymbol{x})\,. \tag{5.11}$$

We remark here that strictly speaking the demonstration above is not completely rigorous. The Poisson summation formula proved previously requires that the function to be in $L^1$, but $G_{free}(\boldsymbol{x})$ is not. The way to circumvent this technical difficulty is to first define the two absolutely convergent series $G_{Fourier}(\boldsymbol{x})$ and $G_{spatial}(\boldsymbol{x})$ as in (5.7) and (5.10). Then, we define $G(\boldsymbol{x}) = G_{Fourier}(\boldsymbol{x}) + G_{spatial}(\boldsymbol{x})$ and simply prove it satisfies the differential equation and the quasi periodic boundary conditions. Notice that $G(\boldsymbol{x})$ is independent of the choice of $\eta$ since $\forall \boldsymbol{x}\in\Omega\backslash\mathbf{0}$,

$$G_{Fourier}(\boldsymbol{x}) + G_{spatial}(\boldsymbol{x}) = \sum_{\boldsymbol{d}\in\Lambda^*}\frac{e^{i\boldsymbol{x}\cdot(\boldsymbol{d}-\boldsymbol{k})}}{|\boldsymbol{d}-\boldsymbol{k}|^2}e^{-\frac{|\boldsymbol{d}-\boldsymbol{k}|^2}{4\eta^2}} + \frac{e^{i\boldsymbol{x}\cdot(\boldsymbol{d}-\boldsymbol{k})}}{|\boldsymbol{d}-\boldsymbol{k}|^2}(1-e^{-\frac{|\boldsymbol{d}-\boldsymbol{k}|^2}{4\eta^2}})\,,$$
$$= \sum_{\boldsymbol{d}\in\Lambda^*}\frac{e^{i\boldsymbol{x}\cdot(\boldsymbol{d}-\boldsymbol{k})}}{|\boldsymbol{d}-\boldsymbol{k}|^2}\,,$$

which is independent of $\eta$.

Next we calculate the singular behaviour of $G(\boldsymbol{x})$ as $\boldsymbol{x} \to \mathbf{0}$. The term $G_{Fourier}(\mathbf{0})$ is finite so this term is readily calculated. However, in the series $G_{spatial}(\boldsymbol{x})$, there is a singularity as $\boldsymbol{x} \to \mathbf{0}$ for the term corresponding to $\boldsymbol{l} = \mathbf{0}$, owing to the fact that the exponential integral $E_1(z)$ has a singularity at 0. Upon using the well-known series expansion of $E_1(z)$

$$E_1(z) = -\gamma - \ln(z) - \sum_{n=1}^{\infty} \frac{(-1)^n z^n}{n n!}\,, \qquad |\arg z| < \pi\,, \tag{5.12}$$

as given in §5.1.11 of [1], where $\gamma = 0.57721\cdots$ is Euler's constant, we derive that

$$F_{sing}(\boldsymbol{x}) \sim -\frac{\gamma}{4\pi} - \frac{\ln\eta}{2\pi} - \frac{\ln|\boldsymbol{x}|}{2\pi} + o(1), \qquad \text{as} \quad \boldsymbol{x} \to \mathbf{0}. \tag{5.13}$$

This shows that $G(\boldsymbol{x})$ has the expected logarithmic singularity as $\boldsymbol{x} \to \mathbf{0}$, and that the regular part of the Bloch Green's function is

$$\begin{aligned} R_{0,\boldsymbol{k}} &= \lim_{\boldsymbol{x}\to\mathbf{0}} \left( G(\boldsymbol{x}) + \frac{1}{2\pi}\ln|\boldsymbol{x}| \right)\,, \qquad (5.14)\\ &= \sum_{\boldsymbol{d}\in\Lambda^*} \frac{1}{|\boldsymbol{d}-\boldsymbol{k}|^2} e^{-\frac{|\boldsymbol{d}-\boldsymbol{k}|^2}{4\eta^2}} + \sum_{\boldsymbol{l}\in\Lambda\setminus\mathbf{0}} e^{i\boldsymbol{k}\cdot\boldsymbol{l}} F_{sing}(\boldsymbol{l}) - \frac{\gamma}{4\pi} - \frac{\ln\eta}{2\pi}\,. \end{aligned}$$

We remark here that if we take conjugate of this expression, we get the same quantity due to the symmetry of the lattice. This gives an alternative proof that $R_{0,\boldsymbol{k}}$ is real-valued. In addition, since $R_{0,\boldsymbol{k}}$ only depends on $\Omega$ and $\boldsymbol{k}$, the expression above should be independent of the choice of $\eta$. To establish this result, we take the derivative of (5.14) with respect to $\eta$ and prove it vanishes. Upon differentiating (5.14), we obtain

$$\frac{\partial}{\partial\eta} R_{0,\boldsymbol{k}} = \sum_{\boldsymbol{d}\in\Lambda^*} \frac{1}{2\eta^3} e^{-\frac{|\boldsymbol{d}-\boldsymbol{k}|^2}{4\eta^2}} - \frac{1}{2\pi\eta} \sum_{\boldsymbol{l}\in\Lambda\setminus\mathbf{0}} e^{-|\boldsymbol{l}|^2\eta^2} e^{i\boldsymbol{k}\cdot\boldsymbol{l}} - \frac{1}{2\pi\eta}\,. \tag{5.15}$$

To show that this expression vanishes, it is equivalent to show that

$$\sum_{\boldsymbol{d}\in\Lambda^*} \frac{\pi}{\eta^2} e^{-\frac{|\boldsymbol{x}-\boldsymbol{d}|^2}{4\eta^2}} = 1 + \sum_{\boldsymbol{l}\in\Lambda\backslash\mathbf{0}} e^{-|\boldsymbol{l}|^2\eta^2} e^{i\boldsymbol{x}\cdot\boldsymbol{l}} = \sum_{\boldsymbol{l}\in\Lambda} e^{-|\boldsymbol{l}|^2\eta^2} e^{i\boldsymbol{x}\cdot\boldsymbol{l}}. \tag{5.16}$$

Notice that the left hand-side is an absolutely convergent series and an integrable function due to the exponential decay. Thus, as we have shown in (2.2), it can be decomposed into a Fourier series of $e^{i\boldsymbol{x}\cdot\boldsymbol{l}}$, where $\boldsymbol{l} \in (\Lambda^*)^* = \Lambda$ and the coefficient of $e^{i\boldsymbol{x}\cdot\boldsymbol{l}}$ is calculated as

$$\begin{aligned}
\frac{1}{|\Omega^*|}\int_{\Omega^*} f(\boldsymbol{y}) e^{-i\boldsymbol{y}\cdot\boldsymbol{l}}\, d\boldsymbol{y} &= \frac{1}{|\Omega^*|}\int_{\Omega^*} \Big(\sum_{\boldsymbol{d}\in\Lambda^*} \frac{\pi}{\eta^2} e^{-\frac{|\boldsymbol{y}-\boldsymbol{d}|^2}{4\eta^2}}\Big) e^{-i\boldsymbol{y}\cdot\boldsymbol{l}}\, d\boldsymbol{y} \\
(\forall \boldsymbol{d}\in\Omega^*,\, \forall \boldsymbol{l}\in\Omega,\, \boldsymbol{l}\cdot\boldsymbol{d} = 2k\pi,\, k\in\mathbf{Z}) &= \frac{1}{|\Omega^*|}\int_{\mathbf{R}^2} \frac{\pi}{\eta^2} e^{-\frac{|\boldsymbol{y}|^2}{4\eta^2}} e^{-i\boldsymbol{y}\cdot\boldsymbol{l}}\, d\boldsymbol{y} \\
(\text{the Fourier transform of a Gaussian}) &= \frac{1}{|\Omega^*|}\frac{\pi}{\eta^2} 4\pi\eta^2 e^{-|\boldsymbol{l}|^2\eta^2} \\
(|\Omega| = 1, \text{ then } |\Omega^*| = 4\pi^2) &= e^{-|\boldsymbol{l}|^2\eta^2}.
\end{aligned}$$

This establishes that $\frac{\partial}{\partial\eta} R_{0,\boldsymbol{k}} = 0$, which yields that $R_{0,\boldsymbol{k}}$ is independent of $\eta$.

The explicit expression (5.14) provides a way to calculate $R_{0,\boldsymbol{k}}$ numerically. Since the two series converge absolutely, for a fixed lattice $\Lambda$ with $|\Omega| = 1$, we can truncate $\Lambda$, $\Lambda^*$ by a finite subset to get a good approximation of $R_{0,\boldsymbol{k}}$. We then minimize it numerically over $\boldsymbol{k} \in \Omega^*\backslash\mathbf{0}$. Notice that Lemma 2 is useful here since it tells us that $R_{0,\boldsymbol{k}}$ blows up as $\boldsymbol{k} \to \mathbf{0}$, thus we can minimize it away from $\mathbf{0}$. Then, we change the lattice and maximize $\mathcal{R}(\Lambda) \equiv \min_{\boldsymbol{k}\in\Omega^*\backslash\mathbf{0}}\{R_{0,\boldsymbol{k}}\}$ over different lattices with $|\Omega| = 1$. The numerical results shown in [8] indicates that $\mathcal{R}(\Lambda)$ is maximized for a regular hexagonal lattice $\Lambda_{op}$ and that $\mathcal{R}(\Lambda^*) = -0.079124$. For a regular hexagonal lattice, Table 5.1 compares the numerical results for the stability threshold, measured in terms of the source strength, and the corresponding one- and two-term asymptotic approximations.

| Lattice | $S_c$ | Leading order | Two term approximation |
|---|---|---|---|
| $\epsilon = 0.1$ | 1.3854 | 1.3603 | 1.3706 |
| $\epsilon = 0.01$ | 0.4306 | 0.4302 | 0.430526 |

Table 5.1: Source strength threshold and its asymptotic approximation for a regular hexagonal lattice with $|\Omega| = 1$ and $f = 0.4$.

## 5.3 Case Study: $N$ Peaks on a Ring

In this section, we implement our stability theory for the finite domain for a particular arrangement of spots inside the unit disk $\Omega = D_1$. We take 5 points $\{\boldsymbol{x}_i\}_{i=1}^5$ equally distributed on a circle of radius 0.5 concentric within the unit disk, as shown in Figure 5.3. The centers of the localized spots corresponds to the locations of these points.

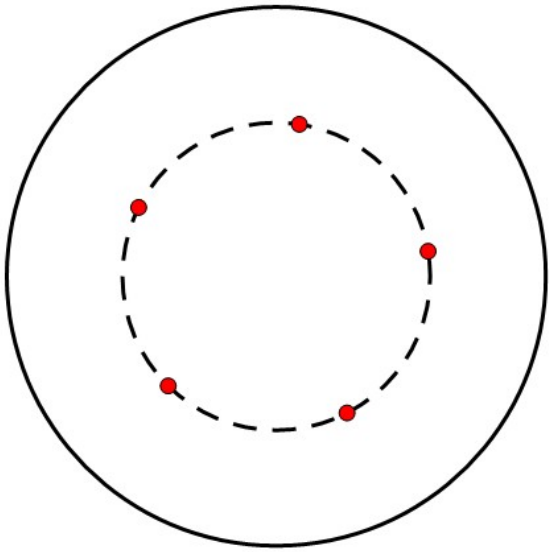

Figure 5.3: 5 localized spots on a ring concentric within the unit disk.

For this special symmetric configuration of 5 equally-spaced spots on a ring, the corresponding Neumann Green matrix $\mathcal{G}$ has a constant row sum, which implies that $\boldsymbol{e}$ is an eigenvector of $\mathcal{G}$. This spot configuration consisting of equally-spaced spots is one of the simplest ways to ensure that

$\boldsymbol{e}$ is an eigenvector of $\mathcal{G}$.

For the unit disk, there is an explicit formula for the Neumann Green's function $G_0(\boldsymbol{x}, \boldsymbol{\xi})$ and its regular part. As derived in [9], we have

$$G_0(\boldsymbol{x}, \boldsymbol{\xi}) = \frac{1}{2\pi}(-\ln|\boldsymbol{x}-\boldsymbol{\xi}| - \ln||\boldsymbol{\xi}|\boldsymbol{x} - \frac{1}{|\boldsymbol{\xi}|}\boldsymbol{\xi}| + \frac{1}{2}(|\boldsymbol{x}|^2 + |\boldsymbol{\xi}|^2) - \frac{3}{4}), \quad (5.17)$$

and thus the regular part $R_0(\boldsymbol{x})$ is given by

$$R_0(\boldsymbol{x}) = \frac{1}{2\pi}(-\ln||\boldsymbol{x}|\boldsymbol{x} - \frac{1}{|\boldsymbol{x}|}\boldsymbol{x}| + |\boldsymbol{x}|^2 - \frac{3}{4}). \quad (5.18)$$

Without loss of generality we label the spot locations $\boldsymbol{x}_i$ on the ring as $\boldsymbol{x}_i = (\frac{1}{2}\cos\frac{2\pi(i-1)}{5}, \frac{1}{2}\sin\frac{2\pi(i-1)}{5})^T$, for $i = 1, 2, ..., 5$. We then substitute this into (5.17) and (5.18) to obtain $\mathcal{G}$. By using Matlab, we numerically calculate all of the eigenvalues of $\mathcal{G}$ as $k_1 = -0.2126$, $k_2 = k_3 = 0.1392$, and $k_4 = k_5 = -0.1174$. Next, we choose the smallest eigenvalue other than the one that corresponding to $\boldsymbol{e}$. This is the eigenvalue $k_4 = k_5 = -0.1174$, which we then use to calculate the stability threshold in terms of the source strength. This allows us to numerically evaluate the second order term in the stability threshold. The full numerical results for the stability threshold, measured in terms of the source strength, are compared versus the one- and two-term asymptotic results in Table 5.2.

| Lattice | $S_c$ | Leading order | Two term approximation |
|---|---|---|---|
| $\epsilon = 0.05$ | 0.9742 | 0.9713 | 0.9619 |
| $\epsilon = 0.02$ | 0.6110 | 0.6083 | 0.6107 |

Table 5.2: The stability threshold in terms of the source strength S and its one- and two-term asymptotic approximation for a 5 spot pattern on a ring of radius 0.5 concentric within the unit disk with $f = 0.4$.

We remark that in this case, there is an analytical way to determine the eigenvalues of the Neumann Green matrix $\mathcal{G}$. Since this matrix is cyclic, its eigenvectors are $\boldsymbol{q}_i = (1, \omega^{i-1}, (\omega^{i-1})^2, ..., (\omega^{i-1})^{n-1})^T$, for $i = 1, 2, ..., n$, while the corresponding eigenvalue is $f(\omega^{i-1})$, where $\omega$ is the $n$-th root of

unity. Here $f(x) = \sum_{k=1}^{n} c_k x^{k-1}$ and $(c_1, c_2, ..., c_n)$ is the first row of $\mathcal{G}$. We can calculate the eigenvalues in this way and obtain the same results as given above by a direct numerical calculation of the eigenvalues by Matlab.

# Chapter 6

# Summary

In this thesis we have studied the linear stability of steady-state localized spot patterns for a singularly perturbed Brusselator reaction-diffusion system in both a periodic and finite domain setting. For both problems, there is a stability threshold $D_c \sim \mathcal{O}(-\frac{1}{\ln \epsilon})$ that characterizes a zero eigenvalue crossing. We have calculated a two term asymptotic approximation for $D_c$ through an asymptotic solution of a singularly perturbed linear eigenvalue problem. In the periodic setting, we first use Floquet-Bloch theory to convert the whole plane problem into a problem posed on a primitive cell together with the Bloch boundary conditions. Then we obtain the leading order approximation for $D_c$ by analyzing a leading order nonlocal eigenvalue problem (NLEP) derived using the method of matched asymptotic expansions. This leading order NLEP is independent of the geometry of the lattice $\Lambda$ and the Bloch vector $\boldsymbol{k}$. In order to characterize the effect of the lattice and the Bloch vector on the stability threshold, we calculated a higher order approximation for $D_c$ by imposing a solvability condition to the next order equations. The calculation leads to a formula for a real-valued continuous band of spectra of the linearization that lies within a small ball near the origin in the spectral plane when $D$ is near the leading order stability threshold. The refined approximation to the stability threshold is obtained from the requirement that this band of spectrum lies in the left half of the spectral plane. The correction to the leading order stability threshold obtained in this way depends on the regular part $R_{0,\boldsymbol{k}}$ of the Bloch Green function, which in turn is determined by the lattice and the Bloch vector $\boldsymbol{k}$. An explicit formula for $R_{0,\boldsymbol{k}}$ is also derived for numerical computation using Ewald summation methods. This formula is used to determine the optimal lattice arrangement which allows for the largest stability threshold.

The analysis for the finite domain problem is similar, with the key difference being that the $N$ spots interact with each other through a Neumann Green matrix $\mathcal{G}$. For a pattern with arbitrarily-located spots, this leads us to analyze $N$ distinct problems, one near each of the spots. For simplicity, we restrict the locations of the spots so that the spots have a common source strength. In this way, the local problem near each of the spots is the same. By decomposing the solution to the linearized problem into the directions of the eigenvectors of $\mathcal{G}$, the analysis becomes very similar to that for the periodic problem. More specifically, we obtain the leading order approximation for the stability threshold through an NLEP that is the same in each of $N-1$ directions. We then calculate the second order approximation by imposing a solvability condition in each direction on the second order terms. This higher order approximation to the stability threshold depends on the matrix eigenvalues of $\mathcal{G}$.

For both the periodic and finite domain problems, we also provide a quick way to derive the stability threshold, which avoids any detailed calculation of spectra near the origin in the spectral plane. This simplified analysis shows that the stability threshold can be determined by solving a nonlinear equation. Numerical comparison between the two-term approximation for the stability threshold in terms of the source strength $S_c$ and the results obtained from solving the nonlinear equation is provided. For the finite domain problem we illustrate our theory for a case study of $N = 5$ equally-spaced localized spots on a circular ring that is concentric with the unit disk.

There are some open problems suggested by this study. Firstly, for the periodic case, numerical evidence obtained from computing the regular part of the Bloch Green's function indicates that it is the regular hexagonal lattice that offers the optimum stability threshold. However, it would be preferable to obtain a rigorous analytic proof of this result. Secondly, although we have employed a systematic asymptotic method to calculate a refined approximation to the stability threshold for the finite domain problem, it would be interesting to extend the rigorous leading-order analysis in [16] to rigorously derive the second order term for the stability threshold.

Thirdly, it would be interesting to try to extend the rigorous framework of [16] to rigorously analyze the periodic problem. The technical difficulty here is that, in contrast to the finite domain problems considered in [16] that have discrete spectra, the periodic problem requires analyzing the edges of a band of continuous spectra. Fourthly, it would be interesting to give a precise relationship between the stability threshold for a multi-spot pattern with regularly spaced spots on a very large but finite domain and that for the periodic problem. It is expected that the stability thresholds for these two problems would be similar, with the only difference being essentially the perturbing effect of a distant domain boundary. More specifically, upon comparing the stability thresholds for the periodic and finite domain problems, we identify a formal correspondence that the regular part of the Bloch Green function $R_{0,\boldsymbol{k}}$ is replaced by the eigenvalues $k_i$ of the Neumann Green matrix. Since we may view the periodic case as the limit of a truncated lattice, i.e. $\Lambda_N = \{n_1\boldsymbol{l}_1 + n_2\boldsymbol{l}_2 | |n_i| \leq N,\ i = 1,\ 2\}$, the question then is how do the matrix eigenvalues $k_i$ approximate, or discretize, the continuous band $R_{0,\boldsymbol{k}}$? Finally, we remark that the analysis in this thesis has focused on determining refined formulae for the stability thresholds associated with $\mathcal{O}(1)$ eigenvalues that result from zero eigenvalue crossings. However, it is well-known that there are additional small eigenvalues of order $\lambda \sim \mathcal{O}(\epsilon^2)$ that are associated with the translation modes. Unstable eigenvalues in this class lead to weak instabilities that are only manifested over very long time intervals. It would be interesting to calculate the stability thresholds for these eigenvalues for both the periodic and finite domain problems. For the finite domain problem, a leading order analysis of these eigenvalues is given in [16] for a related Gierer-Meinhardt reaction-diffusion system.

# Bibliography


[1] M. Abramowitz, I. A. Stegun, et al. *Handbook of mathematical functions*, volume 1. Dover New York, 1972.

[2] G. Beylkin, C. Kurcz, and L. Monzón. Fast algorithms for helmholtz green's functions. *Proceedings of the Royal Society A: Mathematical, Physical and Engineering Science*, 464(2100):3301–3326, 2008.

[3] W. Chen and M. J. Ward. The stability and dynamics of localized spot patterns in the two-dimensional gray-scott model. *arXiv preprint arXiv:1009.2805*, 2010.

[4] X. Chen and Y. Oshita. An application of the modular function in nonlocal variational problems. *Archive for Rational Mechanics and Analysis*, 186(1):109–132, 2007.

[5] B. Gidas, W. M. Ni, and L. Nirenberg. Symmetry of positive solutions of nonlinear elliptic equations in $\mathbf{R}^n$. *Adv. Math. Suppl. Stud. A*, 7:369–402, 1981.

[6] A. Gierer and H. Meinhardt. A theory of biological pattern formation. *Kybernetik*, 12(1):30–39, 1972.

[7] P. Gray and S. K. Scott. Sustained oscillations and other exotic patterns of behaviour in isothermal reactions. *The Journal of Physical Chemistry*, 89(1):22–32, 1985.

[8] D. Iron, John R., M. J. Ward, and J. Wei. Logarithmic expansions and the stability of periodic patterns of localized spots for reaction-diffusion systems in $\mathbf{R}^2$. *Journal of nonlinear science*, submitted.

[9] T. Kolokolnikov, M. S. Titcombe, and M. J. Ward. Optimizing the fundamental neumann eigenvalue for the laplacian in a domain with small traps. *European Journal of Applied Mathematics*, 16(02):161–200, 2005.

[10] T. Kolokolnikov, M. J. Ward, and J. Wei. Spot self-replication and dynamics for the schnakenburg model in a two-dimensional domain. *Journal of nonlinear science*, 19(1):1–56, 2009.

[11] R. Piessens. The hankel transform. *The Transforms and Applications Handbook*, 2:9–1, 2000.

[12] I. Prigogine and R. Lefever. Symmetry breaking instabilities in dissipative systems. ii. *The Journal of Chemical Physics*, 48(4):1695–1700, 1968.

[13] I. Rozada, S. J. Ruuth, and M. J. Ward. The stability of localized spot patterns for the brusselator on the sphere. *SIAM Journal on Applied Dynamical Systems*, 13(1):564–627, 2014.

[14] A. M. Turing. The chemical basis of morphogenesis. *Philosophical Transactions of the Royal Society of London. Series B, Biological Sciences*, 237(641):37–72, 1952.

[15] V. K. Vanag and I. R. Epstein. Localized patterns in reaction-diffusion systems. *Chaos: An Interdisciplinary Journal of Nonlinear Science*, 17(3):037110, 2007.

[16] J. Wei and M. Winter. Spikes for the two-dimensional gierer-meinhardt system: the weak coupling case. *Journal of Nonlinear Science*, 11(6):415–458, 2001.

[17] M. Winter and J. Wei. Existence, classification and stability analysis of multiple-peaked solutions for the gierer-meinhardt system in $\mathbf{R}^1$. *Methods and Applications of Analysis*, 14(2):119–164, 2007.